Title

Interannual differences in sea ice regime in the north-western Barents Sea cause major changes in summer pelagic production and export mechanisms.

Martí Amargant-Arumí[1], Oliver Müller[2], Yasemin V. Bodur[1], Iliana-V. Ntinou[2], Tobias Vonnahme[3], Philipp Assmy[4], Doreen Kohlbach[4], Melissa Chierici[5], Elizabeth Jones[5], Lasse M. Olsen[2,6], Tatiana M. Tsagaraki[2], Marit Reigstad[1], Gunnar Bratbak[2], Rolf Gradinger[1]

[1] Department for Arctic and Marine Biology, UiT – The Arctic University of Norway, Tromsø, Norway

[2] Department of Biological Sciences, University of Bergen, Bergen, Norway

[3] Greenland Climate Research Centre, Greenland Institute of natural resources, Nuuk, Greenland

[4] Norwegian Polar Institute, Fram Centre, Tromsø, Norway

[5] Institute of Marine Research, Tromsø, Norway

[6] Aqua Kompetanse, Flatanger, Norway

Highlights

- Latitudinal structuring of the microbial community in a year with more sea ice.
- High surface primary and bacterial production close to the sea-ice edge.
- High surface vertical flux with strong attenuation profile in year with more sea ice.
- Later seasonal stage of the microbial community due to earlier sea-ice retreat.
- Different microbial communities sustained similar primary production in both years.

Graphical Abstract

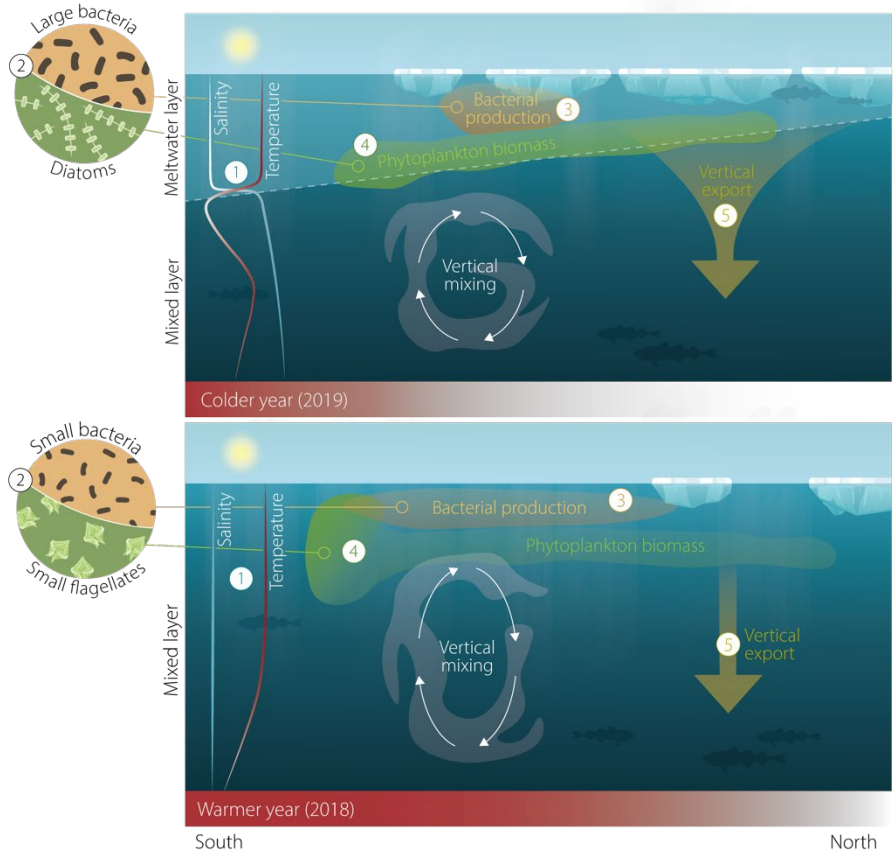

North-western Barents Sea late summer microbial ecosystem

Sea ice conditions in late summer in the north-western Barents Sea are shaping the physical and biological ocean characteristics. In the year with more sea ice, the ocean is more stratified due to a meltwater layer (1) and microbial community composition (2) is structured along a latitudinal gradient, where bacterial (3) and primary production (4) are highest close to the sea-ice edge. In the ice-free summer, the microbial community (2) is in a later seasonal stage and peak production values are found in the southern region (3) (4) of the north-western Barents Sea associated to the AW inflow. In both sea-ice scenarios, primary production values are comparable and while vertical particle flux (5) is higher in the surface in the year with more sea ice, the export is similar in both years.

Abstract

The Barents Sea is a highly dynamic and productive marine ecosystem and a hotspot of global warming. Variability in sea ice extent is a common feature in the Barents Sea with substantial movements of the sea ice edge on short-term, seasonal to interannual time scales. Historically the northern Barents Sea (north of 75ºN) has been ice-covered in winter, but recently it has become the area with most winter ice loss in the Arctic, and year-round ice-free conditions are predicted for the second half of the 21st century. These environmental changes have significant implications for the marine ecosystem. In this study we used contrasting sea ice regimes in August 2018 and August 2019 to explore the response of phytoplankton and bacterial production, microbial abundance, and vertical carbon flux in the north-western Barents Sea (between 76ºN and 83ºN) to the variability of sea ice. While the study area was ice-free in August 2018, extensive areas north of 79ºN were ice-covered in 2019. When the northern parts of the transect were still ice covered, diatoms and other larger phytoplankton were dominant and highest abundances were observed following the receding ice edge. In contrast, under ice-free conditions in 2018, the pelagic ecosystem resembled a post-bloom stage of the seasonal succession with higher abundance of small phytoplankton and heterotrophic protists and low vertical flux throughout the water column. While phytoplankton biomass, bacterial production and downward vertical flux of particulate organic carbon in the upper 60 m were on average higher in 2019, primary production and carbon export below the euphotic layer were comparable between both years. However, overall highest primary production, bacterial production and abundance of both photosynthetic and heterotrophic microorganisms were observed in surface waters (upper 30 m) in 2019, connected to the retreating ice edge, where also vertical particle flux was higher and characterized by a strong attenuation curve. The results clearly demonstrate that differences in ice cover affect the phenology of pelagic primary production and associated biological processes in the Barents Sea.

Introduction

Atmospheric warming drives change in the upper ocean, particularly affecting Arctic marine ecosystems, where temperatures are increasing faster than in any other region in the world (Ingvaldsen et al., 2021; Rantanen et al., 2022). The recent ocean warming and reduced sea ice extent represent climate change effects with broad yet uncertain environmental impacts (Csapó et al., 2021). There is a multitude of predictions on how Arctic marine ecosystems might react to altered conditions, and while still debated, there is consensus that sea ice decline will lead to increased light availability for phytoplankton, and remote sensing data indicate an overall increase of primary production in the Arctic (Ardyna and Arrigo, 2020; Arrigo and van Dijken, 2015; Lewis et al., 2020). However, predictions and processes are not equal for the entire Arctic and there are areas that might experience processes that reduce primary productivity, such as darkening of the upper water column and increased stratification, inhibiting mixing of nutrients into surface waters due to run-off from land (Dunse et al., 2022; McLaughlin and Carmack, 2010; Nummelin et al., 2016; Slagstad et al., 2015 , Konik et al., 2021).

Atlantic Water (AW) inflow regions around Svalbard are hot spots of warming and sea ice reduction, both key consequences of Atlantification of the Arctic (Asbjørnsen et al., 2020; Ingvaldsen et al., 2021). The Barents Sea, particularly affected by Atlantification, is experiencing up to 2.5 times the Arctic warming average and 5 to 7 times the global warming average, which has direct negative effects on sea ice concentrations (Årthun et al., 2019; Isaksen et al., 2022). While ice-free summers are a common feature in the Barents Sea, there are still years when large parts of the northern Barents Sea remain ice-covered in late summer and strong interannual sea ice variability is typical for this Arctic region (Årthun et al., 2019; Bonan et al., 2021; Rieke et al., 2022). Seasonal stratification of the water column, driven by sea-ice meltwater, is typical for the northern Barents Sea. Cold and fresh Polar Water (PW) overlays deeper, saltier and warmer AW transported from the South via the Norwegian Atlantic Current into the southern Barents Sea and via its extension, the West Spitsbergen Current, around Svalbard to the northern part of the Barents Sea. The AW and PW can mix and are modified along their way into the Barents Sea (warm Polar Water [wPW] and modified Atlantic Water [mAW]) (Sundfjord et al., 2020). With less sea ice and reduced freshwater input from sea-ice meltwater, combined with an increased inflow of AW, the seasonal stratification in the northern Barents Sea continues to weaken and will shift the region to Atlantic conditions (Lind et al., 2018). The extent of the sea ice, alongside with the extent of the water masses is variable from year to year and is thereby affecting the distribution of organisms and ecosystem processes, such as primary and bacterial production, in the Barents Sea (Dalpadado et al., 2014; Ingvaldsen et al., 2021; Reigstad et al., 2002).

The environmental conditions in the Barents Sea are major drivers defining seasonal and interannual variability in the ecosystem, including abundance and activity of marine microbes and their interactions in the tightly linked marine microbial food web (MMFW) (Wassmann et al., 2006). Changes in the MMFW have important implications for the marine carbon cycle. Photosynthetic organisms transform CO_2 into organic substrates that are partly re-mineralized by bacteria, transferred to higher trophic levels via grazing or buried at the sea floor. Typical for a high latitude region, phytoplankton biomass in the Barents Sea is low

during winter and early spring and peaks during the spring bloom between mid-April to mid-May in the southern region and following the receding ice edge up until June/July in the northern parts (Kohlbach et al., 2023; Silva et al., 2021). The variability of sea ice cover is critical for the timing of the phytoplankton spring bloom, as light availability and stratification from ice-melt determines the onset of the bloom in ice covered areas (Hunt et al., 2013; Skjoldal and Rey, 1989). In response to the extent and duration of the sea ice cover, both the phytoplankton community composition and the intensity of the blooms can vary (Dalpadado et al., 2020; Dong et al., 2020; Kohlbach et al., 2023; Wassmann, 2011). Typically, after three to four weeks of bloom duration, inorganic nutrients (nitrate, phosphate and silicic acid) become largely depleted and phytoplankton biomass declines due to zooplankton grazing, nutrient limitation, and sedimentation of aggregated cells (Sakshaug et al., 2009). With increasing winds and decreasing stratification in fall, nutrients are resupplied to the surface layer through mixing with sub-surface waters, and a short autumn phytoplankton bloom can be initiated (Dalpadado et al., 2020; Orkney et al., 2022).

This typical succession of phytoplankton production in the northern Barents Sea will be altered with increasing variability of interannual sea ice cover in the future. With a reduction in winter sea ice, larger areas become ice-free earlier in the year, resulting in earlier onsets of phytoplankton growth, but at the same time decreasing the area for sympagic production by ice algae, leading to uncertainties towards primary production in the future ice-free Barents Sea (Campbell et al., 2022; Dalpadado et al., 2020; Kahru et al., 2016; Nøst Hegseth, 1998; Polyakov et al., 2020). Ultimately, both phytoplankton bloom composition and timing, will have, due to different species-specific properties and uncoupling with grazers, consequences for the vertical carbon flux and transfer within the marine food web. The interplay between phytoplankton and heterotrophic bacteria will ultimately shift with changes in nutrient availability and phytoplankton community composition, as specific phytoplankton-bacteria interactions at different stages of the phytoplankton bloom are often linked to specific taxa (Müller et al., 2021; Sapp et al., 2007; Seymour et al., 2017).

In the Barents Sea, stronger AW influence and decreasing sea ice cover are the predominant ecological drivers of the composition and activity of phytoplankton communities, which will ultimately affect other links in the MMFW, with unknown cascading effects on the entire marine ecosystem (Dinasquet et al., 2018; Polyakov et al., 2017; Thingstad, 2020). While this is experimentally difficult to test, understanding the impact of varying ice conditions on the MMFW is important to predict how sea ice change in the future will affect the carbon transfer and export in Arctic marine ecosystems. The Barents Sea, with its large interannual differences in ice cover, is the ideal large-scale simulator to investigate how the ecosystem will respond to changed water mass extents and reduced sea ice cover (Årthun et al., 2019; Bonan et al., 2021; Rieke et al., 2022). The Norwegian Nansen Legacy project provided us with the opportunity to study two summer seasons with highly contrasting sea ice cover, which could serve as representatives for conditions typical for the past ice-covered Barents Sea ecosystem and for how it might change in an ice-free future. We analyzed the productivity of phytoplankton and bacteria and the vertical carbon flux in comparison to the community composition to outline how the MMFW will respond to those two very different sea ice conditions. The following research questions are addressed; How are the different sea ice conditions affecting 1) microbial community structure; 2) primary and bacterial production and 3) carbon export. We hypothesized that the low ice conditions in 2018, with an ice-free

north-western Barents Sea in late summer would be reflected in an ecosystem resembling post-bloom conditions, with a phytoplankton community dominated by small species and a low bacterial carbon turnover. At the same time, with the larger sea-ice extent in August 2019, we expected an ecosystem adjusted to the conditions of melting sea ice, including diatom-dominated phytoplankton communities along the retreating ice edge and higher carbon turnover due to higher primary production. The analysis of this comprehensive dataset enabled us to showcase how variability in sea ice extent impacted the carbon flow within an altered MMFW.

Material and methods

Study Area and Sampling

Within the Norwegian Nansen Legacy project (http://nansenlegacy.org), a transect east of Svalbard in the northern Barents Sea (76ºN to 83ºN) was sampled in August of two consecutive years (2018 - 2019) (Figure 1). The transect followed the complex hydrography of the Barents Sea shelf area into the Nansen Basin of the Arctic Ocean and included stations P1 to P7 (Figure 1). In 2018, stations P6 and P7 were not sampled in order to reach the marginal ice zone for a sea-ice covered station (PICE). Four water masses (Sundfjord et al., 2020) are characteristic for the study area: warmer and saltier Atlantic Water (AW) and modified Atlantic Water (mAW), colder and fresher Polar Water [PW] and warm Polar Water (wPW), and deeper Intermediate Water (IW). Atlantic Water masses are transported via the Norwegian Atlantic Current into the southern part and via the West Spitsbergen Current around Svalbard into the northern part of the Barents Sea. A detailed characterization of the hydrography of the study area can be found in Ingvaldsen and Loeng (2009) and Lundesgaard et al. (2022).

Seawater samples were taken during the Nansen Legacy Joint Cruise 1-2 (from August 6th to 23rd in 2018; cruise 2018707 (Ingvaldsen et al., 2020); CTD: https://doi.org/10.21335/NMDC-714672628) and Seasonal Cruise Q3 (from August 5th to 27th in 2019; cruise 2019706 (Reigstad et al., 2022); CTD: https://doi.org/10.21335/NMDC-1107597377) onboard the ice breaker RV *Kronprins Haakon*, using a CTD (Seabird SBE 9 CTD unit) rosette equipped with 24 x 12 L Niskin bottles following the Nansen Legacy protocol (further details regarding sensors and individual sampling procedures can be found here: ((Nansen Legacy, 2022); https://arvenetternansen.com/report-series/). The CTD rosette was deployed either from the side of the ship or through a moon pool, depending on sea ice conditions, which influenced upper sampling depth (5 m when deployed from the side and 10 m when deployed through the moon pool). Standard depths were 5, 10, 20, 30, 40, 50, 60, 90, 120, 200, 500, 1000, 2000 m and variable depths included deep chlorophyll maximum (DCM) and 10 m above the sea floor. The daily sea ice concentrations at Nansen Legacy stations in 2018 and 2019 were retrieved from published datasets (https://doi.org/10.21334/npolar.2023.24f2939c) which were derived from AMSR-2 and AMSR-E sea ice concentrations products. The sea ice concentration data was then transformed to represent presence or absence of sea ice contrasting the two years (Figure 2).

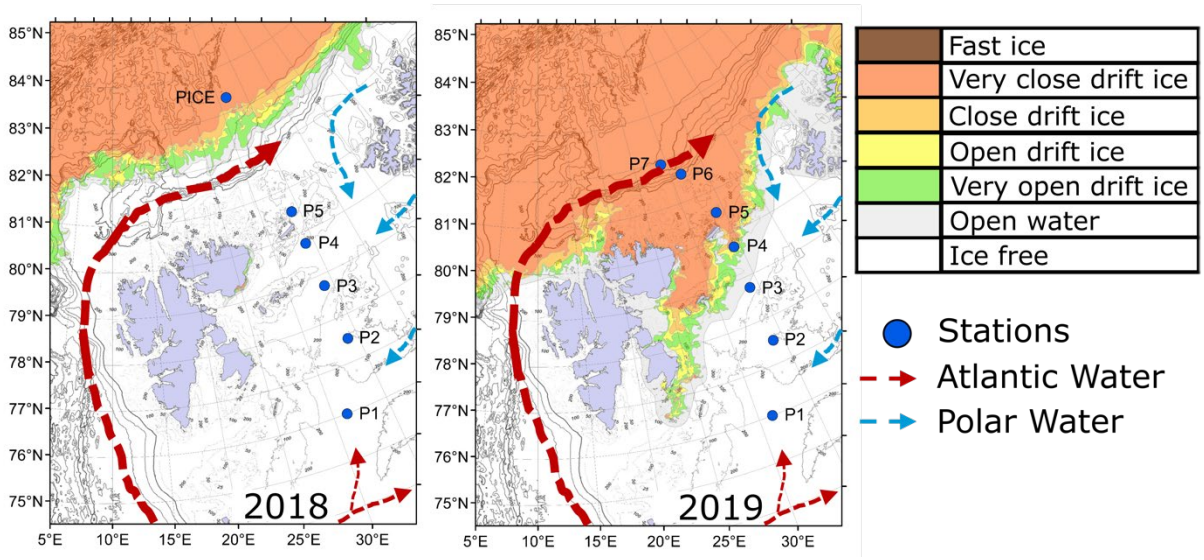

Figure 1: Map of the study area, showing the sampling stations (P1-P7/PICE), simplified Atlantic Water and Polar Water inflow directions (red and blue dashed arrows) and sea ice extent in August 2018 (left) and August 2019 (right). Ice data are from 15.08.2018 and 15.08.2019 and were provided by the Norwegian Ice Service - MET Norway. The ice concentration categories refer to following sea ice concentrations: 100 %: Fast ice; 90-100 %: Very close drift ice; 70-90 %: Close drift ice; 40-70 %: Open drift ice; 10-40 %: Very open drift ice; 0-10 %: Open water; 0 % Ice free. Bathymetry: NOAA National Centers for Environmental Information; International Bathymetric Chart of the Arctic Ocean; General Bathymetric Chart of the Oceans.

Inorganic nutrients and photosynthetically active radiation

Samples for measurements of the macro-nutrients nitrate [NO_3^-], nitrite [NO_2^-], phosphate [PO_4^{3-}], and silicic acid [$Si(OH)_4$] were filled into 20 mL vials, preserved with 250 µL chloroform and stored in the dark at 4 °C. Post-cruise analysis was performed using colorimetric methods (Grasshoff et al., 1978; Gundersen et al., 2022) at the Institute of Marine Research, Bergen, Norway. The detection limits were 0.5 mmol m^{-3} for [NO_3^-], 0.06 mmol m^{-3} for [PO_4^{3-}] and 0.7 mmol m^{-3} [$Si(OH)_4$]. Nutrient data for each of the cruises can be found in Chierici et al. ((2021a), https://doi.org/10.21335/NMDC-839276558; (Chierici et al., 2021b), https://doi.org/10.21335/NMDC-1472517325).

Photosynthetically active radiation (PAR, µmol photons m^{-2} s^{-1}) was measured using a Biospherical Li-cor Chelsea sensor mounted on the CTD rosette (2018: https://doi.org/10.21335/NMDC-714672628; (Ingvaldsen, 2022); 2019: https://doi.org/10.21335/NMDC-1107597377; (Reigstad, 2022)). For stations in which the rosette was deployed from the side of the ship (all stations in 2018 and station P1 in 2019), the direct output of the sensor was reported. In stations in which the rosette was deployed through the ship's moon pool, the shadow of the vessel was assumed to affect the light measurements until 25-30 m depth. In such cases, a Beer-Lambert curve was fitted on the data points ranging between the impacted depths and the detection limit of the sensor, assuming constant attenuation. The resulting equations were used to estimate irradiance in the uppermost (25-30 m) water column. For the sea ice-covered stations, a light transmittance of 4 % under summer first-year ice with <10 cm of snow covered was assumed (Nicolaus et al., 2012) in order to estimate the irradiance incident on the sea-ice surface. An

average between the above numbers, using the ice-cover proportion as weighing factor, was calculated to obtain a representative surface irradiance at each station. For all stations, the depth at which irradiance was 1 % of the surface irradiance was considered to be the limit of the euphotic zone (Table A2).

Biogeochemical variables

Suspended particulate organic carbon (POC)

The sampled water was placed into plastic bottles which were stored in the dark at 0-2 °C and processed within 4 hours. Between 0.05 and 2 L of the sample was filtered onto pre-combusted Whatman GF/F filters using low vacuum pressure (-30KPa), depending on the coloration of the filter. The filters were then folded, wrapped in pre-combusted aluminum foil and frozen at -20 °C until analysis. The filters were dried overnight at 60 °C, and afterwards acid-fumed with hydrochloric acid for 24 h before they were dried again for 24 h at 60 °C. Subsequently, they were packed in tin capsules and the 2018 dataset ((Bratbak et al., 2022); https://doi.org/10.11582/2022.00049) was measured with a Flash 2000 Organic Elemental Analyzer (Thermo Scientific) and the 2019 dataset ((Marquardt et al., 2022); https://doi.org/10.11582/2022.00055) with a CE440 Exeter Analytical CHN analyzer.

Chlorophyll *a* (Chl-*a*) and phaeopigments

Water samples were stored in plastic containers in the dark at 0-2 °C and processed after no longer than 1 hour. Between 0.15 and 1 L of the sampled water was filtered onto Whatman GF/F 25 mm filters using low pressure vacuum. The filters were transferred to polypropylene tubes and 5 mL of methanol were added to extract the pigments. Extraction took place over 24 h at 4 °C. Chlorophyll *a* and phaeopigments concentration was determined according to Holm-Hansen and Riemann (1978) with a Turner Design AU10 fluorometer. The photopigment data for both cruises can be retrieved from (Vader et al., 2021; https://doi.org/10.21335/NMDC-1371694848). All filtration, extraction, and measurement steps were performed in the dark.

Elemental concentrations of particulate matter (XRF analysis)

For the total particulate element analysis three replicates of approximately 1.5 L from each water sample were filtered on Whatman® Nuclepore™ polycarbonate (PC) filters, 47 mm in diameter, 0.6 µm pore size, using ≤200 mmHg vacuum pressure. After filtration, each filter was rinsed with 5 mL of distilled water to prevent interference from salt crystals, then left to air-dry and kept dry in petri slides until further analysis. Total particulate concentrations of P, S, Ca, O, Si, Fe and Mn were measured by wavelength dispersive X-Ray fluorescence spectroscopy (WDXRF) in a Bruker® AXE S4 pioneer XRF instrument. The concentrations for the above-mentioned chemical elements were calculated based on the calibration parameters and detection limits explained in Paulino et al. (2013). The instrument provides a bulk amount of particulate element concentration and does not discern between different chemical forms. At least three blank filters from each new batch and three filters with filtered distilled water were analyzed for reference prior to analyzing the samples. The data for both cruises can be found at NMDC (Tsagkaraki et al., 2023) ;2018:

https://doi.org/10.21335/NMDC-1663991306-2018707; 2019: https://doi.org/10.21335/NMDC-1663991306-2019706).

Flow cytometry

For the measurement of the abundance of viruses, bacteria (the term "bacteria" is used throughout the paper, because archaea were nearly absent (< 1 %; Thiele et al., this special issue) in the euphotic zone during our sampling period), pico- and nanophytoplankton and heterotrophic nanoflagellates (HNF), water samples of 1.8 mL were taken as triplicates, fixed with 36 µL 25 % glutaraldehyde (0.5 % final concentration) for 2 h at 4 °C, flash-frozen in liquid nitrogen and stored at -80 °C until analysis. Abundances of pico- and nanosized phytoplankton, as well as HNF, were determined using an Attune® Acoustic Focusing Flow cytometer (Applied Biosystems by Thermo Fisher Scientific, Waltham, MA, USA)) with a syringe-based fluidic system and a 20-mW 488-nm laser. For the measurement of HNF abundance, the samples were stained with SYBR Green I (SYBR Green I; Molecular Probes, Eugene, OR, USA) for 2 h in the dark, and subsequently, 1.5 mL were measured at a flow rate of 500 µL min^{-1} following the protocol of Zubkov et al. 2007. Autotrophic microorganisms were counted directly after thawing, and the different phytoplankton groups were discriminated based on their red fluorescence (BL3) vs. orange fluorescence (BL2) (Figure A7 and Paulsen et al. (2016)). For the measurement of virus particles and bacteria, a FACS Calibur (Becton Dickinson) flow cytometer was used. Prior to analysis, samples were first thawed, diluted 10 times with 0.2-µm-filtered TE buffer (Tris 10 mM and EDTA 1 mM, pH 8), stained with a green fluorescent nucleic acid dye (SYBR Green I) and incubated for 10 min at 80 °C in a water bath (Marie et al., 1999). The stained samples were counted at a low flow rate of around 60 µL min^{-1} and different groups discriminated on a biparametric plot of green fluorescence (BL1) vs. side scatter (SSC). This allowed to distinguish virus particles (mainly DNA containing) of different sizes (Larsen et al., 2008), and different bacterial groups including low nuclear acid (LNA) and high nuclear acid (HNA) bacteria. The data for both cruises can be found at NMDC (Müller et al., 2023b; 2018: https://doi.org/10.21335/NMDC-753383895; 2019: https://doi.org/10.21335/NMDC-39569968).

Rate measurements: NPP, BP and vertical flux

Net primary production (NPP) rates were estimated using the ^{14}C uptake technique on *in situ* incubations. Water subsamples were collected at discrete depths from a CTD rosette. The samples were collected in dark plastic bottles and stored in the dark at 0-2 °C until processing, no longer than 1 h. 250 mL from each depth were transferred to one light and one dark polystyrene bottle. $NaH^{14}CO_3$ was added to the incubation bottles to a final activity of 0.1 mCi/mL. Two 250 µL subsamples were taken from each incubation bottle and fixed with 250 µL pure ethanolamine to determine the total concentration of added carbon. The bottles were deployed at the corresponding sampling depths using a mooring rig that drifted freely, either floating in open water or tethered to an ice floe. The bottles were retrieved after 18-25 hours. The contents of the bottle were filtered onto 25 mm Whatman GF/F filters using low pressure vacuum in the dark. After filtration, the filters were placed in 20 mL scintillation vials and 750 µL concentrated HCl was added and the vials incubated for 24 hours, after which

the vials were ventilated to remove all non-fixed inorganic carbon. 10 mL of scintillation cocktail (Ecolume) were added prior to the analysis of the samples in a Tri-Carb 2900TR liquid scintillation counter (PerkinElmer). Samples were counted for 10 minutes, and an average of three counts was taken.

Bacterial production (BP) was calculated based on the method of the incorporation of 3H-leucine according to Smith & Azam (Smith and Azam, 1992). Water samples of 50 mL were taken from Niskin bottles and four replicates of 1.5 mL were transferred to 2 mL Eppendorf vials. One replicate served as control, where 80 µL of 100 % trichloroacetic acid (TCA) were immediately added. All replicates were incubated with 25-nM 3H-leucine (final concentrations) for 2 h at *in situ* temperature, and the incubations were stopped by adding 80 µL of 100 % TCA. Before analysis, samples were centrifuged for 10 min at 14,800 rpm, the supernatant was removed and the pellet subsequently washed with 1.5 mL 5 % TCA. This step was repeated twice and after the third centrifugation round and the supernatant was removed, 1.5 mL of scintillation liquid (Ultima Gold) was added and the radioactivity in the samples was counted on a Perkin Elmer Liquid Scintillation Analyzer Tri-Carb 2800TR. The measured leucine incorporation was converted to µg carbon incorporated per L per day (presented as mg C m^{-3} d^{-1}), using the specific activity of the isotope and the constant 1797 (grams of protein produced per mole of incorporated leucine) and 0.86 (the weight ratio (g:g) of total C:protein in bacteria) according to Simon & Azam (Simon and Azam, 1989), which gives a conversion factor of 1.5 kg C per mole of incorporated leucine, assuming no isotope dilution (Kirchman et al., 2009a). The data for both cruises can be found at NMDC (Müller et al., 2023a); 2018: https://doi.org/10.21335/NMDC-1815353537-2018707; 2019: https://doi.org/10.21335/NMDC-1815353537-2019706).

In order to determine the downward vertical flux of particulate organic carbon and particulate nitrogen (POC/PON), drifting short-term sediment traps (KC Denmark, aspect ratio >6) were deployed at 6 different depths (30, 40, 60, 90, 120 and 200 m), equipped with 2-4 cylinders at each depth at stations P1, P2, P4, PICE1 during August 2018, and at stations P1, P4, P5, P6, P7 during August 2019. Deployment times varied between 18 25 h. Prior to the deployment, sediment traps were filled with filtered (Whatman, GF/F) saline deep water taken at the beginning of each station. After retrieval, the water from the tubes of each depth was pooled and kept dark at 4 °C while it was subsampled for POC within 20h after retrieval. POC was filtered onto pre-combusted (7h, 450 °C) GF/F filters and filters were stored at -20 °C before further processing. Subsequent processing was done in the same way as suspended POC. The data for both cruises can be found at NIRD (Bodur et al., 2023a, 2023b; 2018: https://doi.org/10.11582/2023.00092; 2019: https://doi.org/10.11582/2023.00093).

Statistical analysis

A set of multivariate statistics tools were used to reduce the large dimensionality of the dataset. Unconstrained analyses (principal component analyses) were employed to describe the environmental setting of the study. Constrained analyses were used to test the effects of environmental variables on community composition (canonical correspondence analysis) and carbon flux variables. All multivariate analyses were performed using the “vegan” package in R (Oksanen et al., 2022).

A principal component analysis (PCA) was performed on a subset of the environmental variables (temperature, salinity, PAR, NO_3^-, NO_2^-, $Si(OH)_4$, PO_4^{3-}, Chl-*a* and POC), to visualize the parameter combinations in which the MMFW components were found at the time of sampling and aid with interpretation.

The effect of the environmental variables on the microbial community composition was assessed by Canonical Correspondence Analysis (CCA). Temperature, salinity, PAR, NO_3^-, NO_2^-, $Si(OH)_4$, Chl-*a* and POC were defined as environmental constraints; the abundance of a range of microbial food web members was used as response variables. Both explanatory variables and response variables were standardized by subtracting the mean of each variable from each measurement and dividing the result by the variable's standard deviation (z-scoring). To address non-linearity in the relationships between variables, the explanatory variables dataset was log-transformed. The significance of the canonical axes and the constraints' effects was tested using a Monte Carlo permutation test of 999 permutations.

The influence of potential environmental drivers on carbon flux processes was estimated by a Redundancy Analysis (RDA) using initially the same explanatory variable set as for the CCA. Net primary production rates, bacterial production rates and vertical POC fluxes were computed as response variables. The co-correlation between explanatory variables was assessed and a selection was made between those which had an R^2 value higher than 0.8. A regression coefficient higher than 0.8 was found in the pairs formed by Chl-*a* and phaeopigments, nitrate and silicic acid, nitrate and phosphate, and silicic acid and phosphate. Of these, nitrate (NO_3^-), silicic acid ($Si(OH)_4$) and chlorophyll *a* (Chl-*a*) were retained. An exception to this selection criteria was the $Si(OH)_4$ variable, which had a high correlation coefficient with other macronutrients such as NO_3^- or PO_4^{3-}, but the variation of which is highly relevant to interpret community composition as it pertains to diatom presence. A subsequent RDA was performed with the remaining environmental variables, namely temperature, salinity, PAR, NO_3^-, NO_2^-, $Si(OH)_4$, Chl-*a* and POC. The significance of the canonical axes and the constraints were determined using a Monte Carlo permutation test of 999 permutations. Both RDA and CCA were carried out using the "vegan" package in R (Oksanen et al., 2022). Post-hoc, multiple regression models were fitted for NPP, BP and vertical carbon flux, using the above environmental variables as predictors. Model selection was performed by backward stepwise selection based on the Akaike Information Criterium (AIC). Model selection was carried out using the "MASS" package in R (Venables and Ripley, 2018).

Using the software GraphPad Prism version 9.5.1 for Windows (GraphPad Software, USA, www.graphpad.com) a paired t-test was performed on the environmental variables PAR (n=248), nitrate (n=45) and chlorophyll *a* (n=42), as well as production estimates (net primary production (n=10) and bacterial production (n=38)) and POC flux (n=14) of the upper 120 m comparing 2018 and 2019. A Wilcoxon signed-rank test was performed to compare differences between 2018 and 2019 in nitrate and temperature (n=39) and Chl-*a* and temperature (n=42). Linear regression analyses were performed to compare for each 2018 and 2019 the relationship between Chl-*a* and bacterial production, Chl-*a* and primary production and bacterial production and primary production (Figure A2). Abundances of relevant microbial functional groups, as well as Chl-*a*, POC and carbon flux variables (NPP, BP and vertical POC flux) were integrated over the uppermost 90 m of the water column using a trapezoidal formula (Table A1).

To assess the significance of differences of the measured element concentrations between the two years, a Welch's ANOVA test together with a pairwise t-test was performed. P-values were adjusted using the Bonferroni correction (Armstrong, 2014). The distribution patterns are depicted in section plots using the algorithm Multilevel B-spline Approximation (MBA) for data interpolation. A series of Pearson correlation tests were performed with the Bonferroni correction method to uncover any correlations between the elemental concentrations and the microbial group abundances. The correlation coefficient (a) for any response-predictor relationship was set at a level of $|a| > 0.3$ to account for the number of comparisons being performed. The scripts for all the statistical analyses in R can be retrieved at https://github.com/marti-uit/Summer-Carbon-paper.

Results

Physical characterization of the study area in August 2018 vs. 2019

The two cruises in August 2018 and 2019 displayed very different patterns of sea-ice extent in the north-western Barents Sea during both years (Figures 1 and 2). In 2018, the entire transect was mostly ice-free from June until November, while in 2019 the northern stations P5 to P7 were ice covered for most parts of the year including summer. From January to April, the ice edge in both years was located between stations P3 and P4, however in 2018, from the end of January until mid-March, large open water areas formed in the northern parts of the transect.

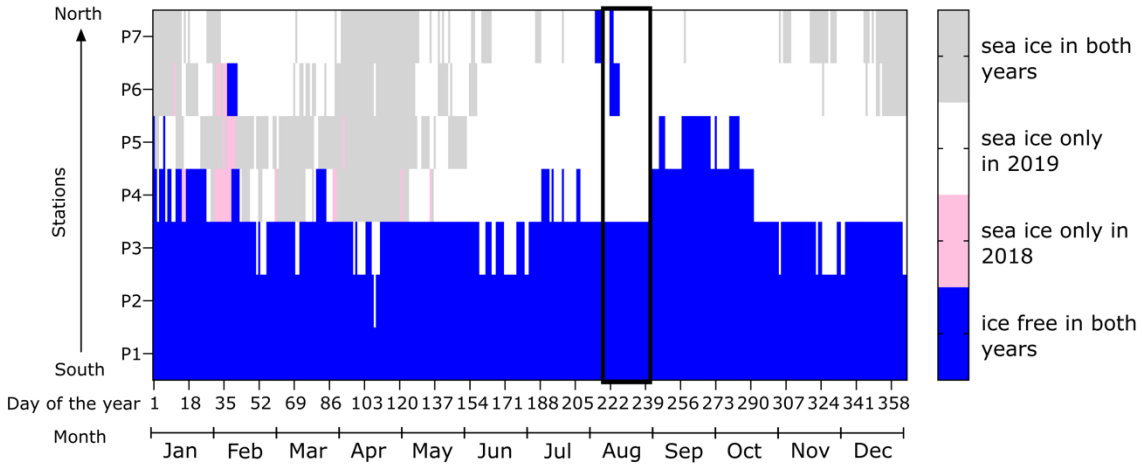

Figure 2: Differences in sea ice extent between 2018 and 2019 (in presence/absence) at the stations of the transect in the Barents Sea (76ºN – 82ºN). The black box highlights the sampling period (the northernmost station in 2018 (PICE) is not included in this figure).

Besides differences in sea ice extent, also the contribution of water masses, as evident in salinity and temperature changes, differed between the two years (Figure 3 and 4A; Figure A1). The upper 120 m of the water column at stations P1-P5 were both colder and fresher in 2019 compared to 2018. Temperature differences between the two years were significant (t-test, $p<0.0001$, $n=47$) and especially pronounced in the upper 40 m (up to 5 °C colder between

5-20 m in 2019) and closer to the surface with decreasing distance to the ice edge (Figure 4A). The temperature and salinity changes between the two years were also apparent in the extent of either AW or PW influenced water masses (Figure 3). In 2018, when temperatures were higher, wPW was with 40 % (as average over the upper 120 m of all stations) more abundant compared to 2019 (30 %, Figure 3B). At the same time, the PW was less abundant in 2018 (48 %) than in 2019 (65 %). AW was only encountered in the upper 120 m in 2018 at station P1, while in 2019 it was mAW. In 2018, AW was found at stations P1 (between 30 and 150 m) and PICE (between 170 and 230 m), corresponding to the southern and northern inflow of AW into the Barents Sea (Figure 1 and 3A), while in 2019, AW was only detected at the northernmost station P7 (between 150 and 400 m) and predominantly mAW at station P1.

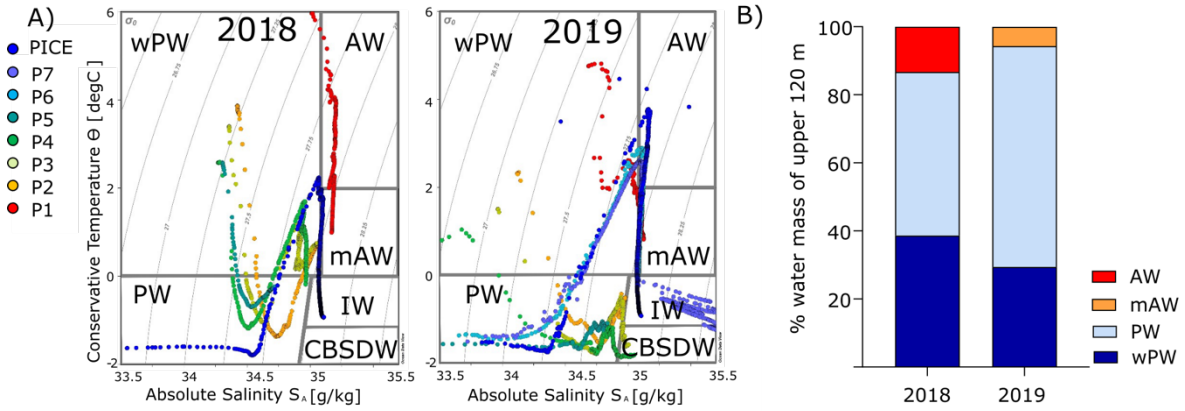

Figure 3: A): TS-plots of CTD profiles at the process stations (P1-P7/PICE) in August 2018 (left) and August 2019 (right) and the corresponding water masses. B): average abundance of water masses over the upper 120 m of all stations for 2018 and 2019. AW: Atlantic Water; mAW: modified Atlantic Water; PW: Polar Water; wPW: warm Polar Water; IW: Intermediate Water; CBSDW: cold Barents Sea Dense Water. Water mass definitions are according to Sundfjord et al. (2020).

In addition to the observed differences in sea ice extent (Figure 2) and water mass distribution (Figure 3), other environmental variables, such as PAR and nitrate concentrations in the upper 120 m were significantly different (PAR: t-test, $p<0.0001$, $n=248$; NO_3^-: t-test, $p=0.006$, $n=45$) between the two years (Figure 4B and C and Figure A1). In 2018 PAR levels were higher and reached deeper waters than in 2019 (except at station P1, Figure 4B), while nitrate concentrations were higher in 2019. Largest interannual differences were observed closer to the surface with decreasing distance to the ice edge (Figure 4C). Following a similar pattern as nitrate, the phytoplankton biomass (Chl-*a* concentrations) was significantly higher (Chl-*a*: t-test, $p<0.0001$, $n=42$) in 2019 compared to 2018 (Figure 4D and SI 1). From station P2 at 40-50 m and northwards, the largest differences in phytoplankton biomass between 2019 and 2018 were found closer to the surface with decreasing distance to the ice edge. For both nitrate and Chl-*a*, the differences observed between 2018 and 2019 correlated significantly with differences in temperature (Wilcoxon signed-rank test, $p<0.0001$) for our sampling transect, with the observed trend of larger differences with closer distance to the ice edge (Figure 4C and D).

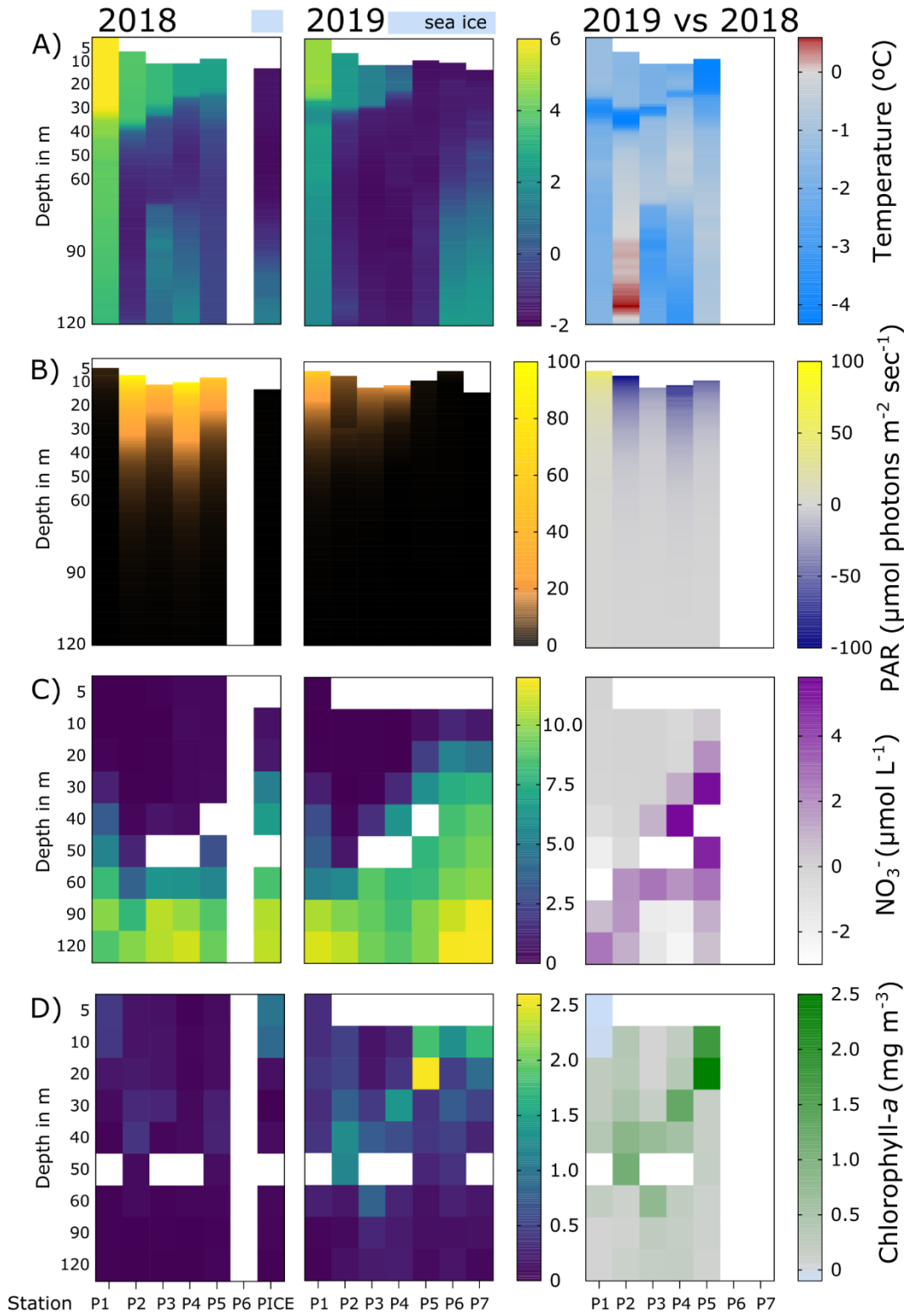

Figure 4: Comparison of A) sea water temperature, B) photosynthetically active radiation (PAR), C) nitrate (NO_3^-) and D) chlorophyll *a* (Chl-*a*) concentration at the stations for the upper 120 m of the water column from August 2018 and 2019, where differences from 2019 compared to 2018 are indicated on the right panel. White background indicates that samples were not taken in one of the

years, station P6 and P7 were not sampled in 2018. The sea ice extent for the respective years is indicated with blue bars on top of the panels. Note the different depth-scales for the plots (continuous for CTD-sensor data, temperature and PAR and discrete for NO_3^- and Chl-*a*).

Figure 5 summarizes the relationships between the environmental drivers using a principal component analysis ordination plot. The first two principal components (PCs) explained 72.3 % of the variance in the sampled locations. PC1 explained 45.2 % and PC2 (temperature, salinity, PAR, Chl-*a*) explained 27.2 % of the observed variation. The first PC was correlated to higher levels of nutrients, and lower values in POC, Chl-*a* and PAR. The second PC was most strongly correlated with higher temperatures and salinity, largely separating the PW mass in 2019 from all the AW, mAW and wPW masses. PW also showed the highest spread in the ordination, largely driven by the relative contribution of Chl-*a*. All AW and mAW locations belonged to the "high nutrients, low biomass" area of the biplot, whereas the wPW was spread along this gradient in both years and formed two distinct clusters.

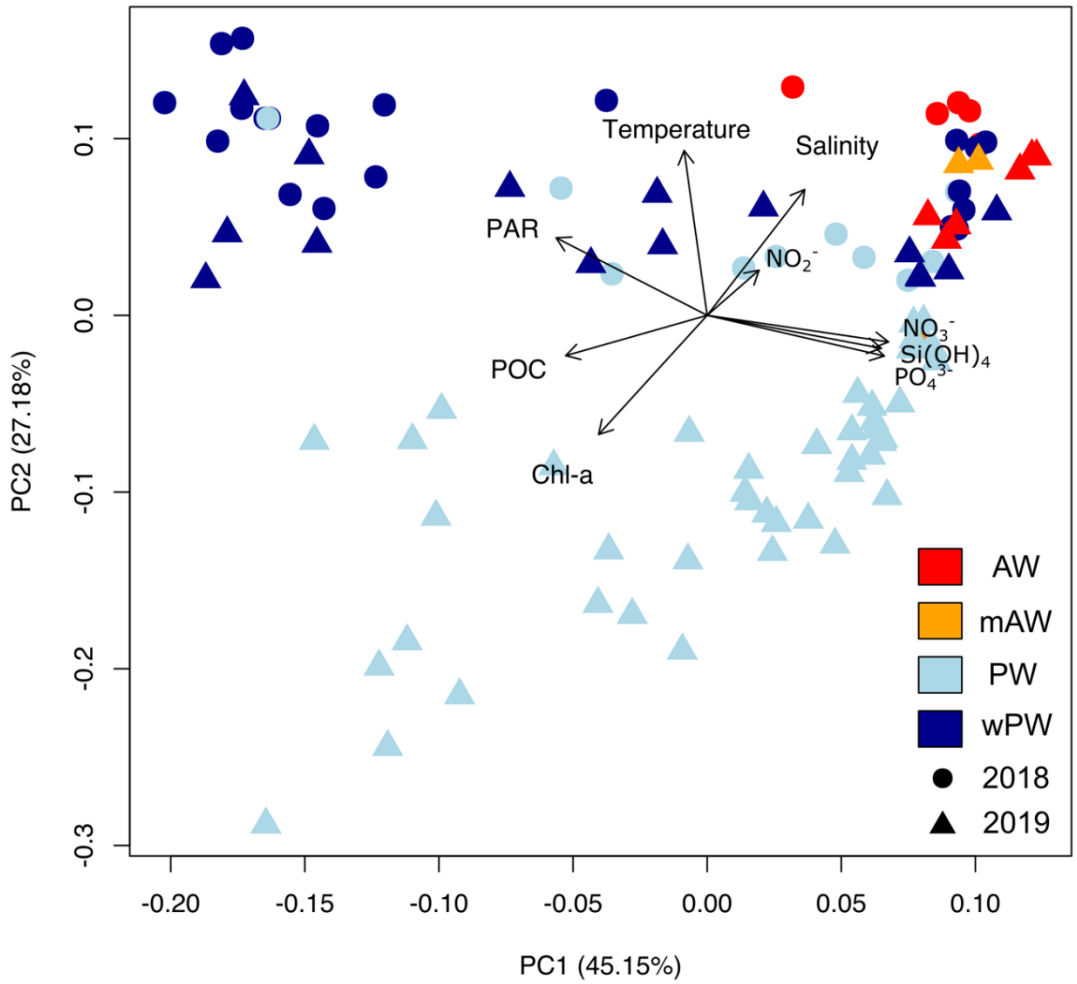

Figure 5: Visualization of the principal component analysis (PCA) of environmental variables of all samples from August 2018 (circle) and 2019 (square), including salinity, temperature,

photosynthetically active radiation (PAR), nitrate (NO_3^-), nitrite (NO_2^-), silicic acid ($Si(OH)_4$), suspended particulate organic carbon (POC) and chlorophyll *a* (Chl-*a*).

Microbial abundance and productivity

The abundance and activity of microorganisms were, as seen for the environmental variables, different between the two years (Figure 6 and 7 and Figure A1). Bacterial abundance showed a similar pattern as described for Chl-*a*, with the majority of sampling points in the upper 120 m of the water column having higher values in 2019 than 2018. Bacterial abundances in surface samples from 2019 ranged between $1.6*10^5$ (P1) and $2.3*10^6$ (P5) bacteria mL^{-1}. In 2018, bacterial abundances ranged between $2.5*10^5$ (P2) and $9.2*10^5$ (P3) bacteria mL^{-1}, respectively. Stations P1 and P5 showed an opposite pattern with higher bacterial abundance in 2018 above and below 50 m, respectively, which was mainly attributed to differences in the HNA (high nucleic acid bacteria) sub-type. Overall, HNA-bacteria were in both years more abundant than LNA (low nucleic acid)-bacteria, but the differences were more pronounced in 2018 (three times more abundant), even though overall abundances of both LNA- and HNA-bacteria were higher in 2019. In 2018, abundances of the HNA subtype ranged between $1.7*10^5$ and $3.4*10^5$ bacteria mL^{-1} and in 2019 between $1.5*10^5$ and $5.6*10^5$ bacteria mL^{-1}. The highest abundance differences (>$5.0*10^5$ cells mL^{-1} difference) were following the Chl-*a* maximum, with the HNA sub-type as the main contributor to the differences. The LNA sub-type showed the highest abundance differences, with higher abundances in 2019, in the surface samples at stations P2, P3 and P5.

In contrast to bacteria, heterotrophic nanoflagellates (HNF) and picophytoplankton had higher abundances in 2018 than 2019 with a few exceptions. Highest picophytoplankton values in 2019 were measured in surface samples from stations P3, P4 and P5, with ~7000-8000 cells mL^{-1}. Abundances were higher in 2018, with highest values in surface samples from stations P4 and P5 of ~11000-12500 cells mL^{-1}. In contrast to picophytoplankton, nanophytoplankton abundances showed a similar pattern as bacterial abundances, overall higher in 2019, with specific peaks at the Chl-*a* maximum and one additional peak at station P1 at 50 m, mainly due to high abundance (~1500 cells mL^{-1}) of large nanophytoplankton (5-10 µm). The highest measurement in 2018 was from surface samples at station P1 with up to ~2000 cells mL^{-1}, of which 75 % was contributed by small nanophytoplankton (2-5 µm), while in 2019 only up to 500 cells mL^{-1} were found at the surface of station P1. In 2019, the highest value of nanophytoplankton was measured at the surface of station P5 with over 3000 cells mL^{-1}, and abundances exceeded 2000 cells mL^{-1} in surface samples from stations P2, P4, P5 and P7. Both smaller and larger nanophytoplankton groups were more abundant in 2019 (Figure A4; 10 (3 in 2018) samples with > 1000 cells mL^{-1} of small nanophytoplankton and 13 (0 in 2018) samples with > 500 cells mL^{-1} of large nanophytoplankton). However, small nanophytoplankton were compared to large nanophytoplankton relatively more abundant in 2018 (between 4-20 times) than in 2019 (between 1-4 times).

Virus abundances showed overall a similar pattern in 2018 and 2019, with higher abundances in surface waters and values ranging between $1.6*10^6$ (P6/P7/PICE) and $1.1*10^7$ (P1/P4) viruses mL^{-1}. However, when comparing the three virus size classes (small, medium, large), there were clear differences between the two years (Figure A5). In 2018, small viruses were more abundant, mainly at stations P1 to P5 and in the upper 60 m, while in 2019, the medium

and large sized viruses were dominant and up to three times more abundant. Their abundance followed in 2019 a similar pattern as seen for Chl-*a* concentrations, with higher abundances of large viruses closer to the surface with decreasing distance to the ice edge, with the exception of low values at station P5 and P6, where high Chl-*a* concentrations were measured. In 2019, the abundance of large virus correlated positively (R^2=0.22, p<0.001) with the abundance of large nanophytoplankton, while in 2018 no significant correlation (R^2=0.02, p=0.28) was detected (Figure A8).

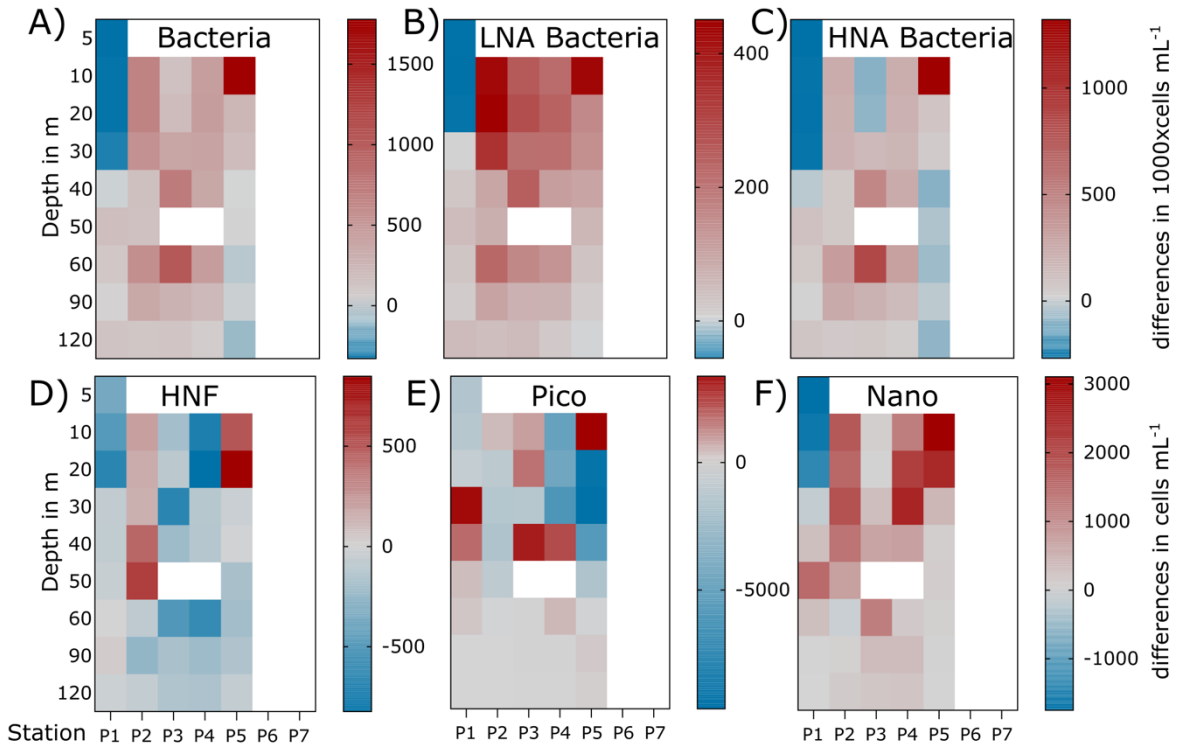

Figure 6: Comparison of abundances of different microbial groups within the upper 120 m of the water column between August 2018 and 2019 (red indicates higher and blue lower values in 2019 compared to 2018, white indicates that comparison was not possible as either 2018 or 2019 was not sampled, stations P6 and P7 were not sampled in 2018). Upper panel from left to right, A) bacteria, B) low-nucleic-acid (LNA) bacteria and C) high-nucleic-acid (HNA) bacteria, with differences presented as 1000xcells mL^{-1}. Lower panel shows from left to right D) heterotrophic nanoflagellates (HNF), E) picophytoplankton (Pico) and F) nanophytoplankton (Nano), with differences presented as cells mL^{-1}.

The described microbial abundance differences were largely reflected in the differences of the microbial productivity in the two contrasting years (Figure 7A and B). Bacterial production (BP) ranged from 0 to 2 mg C m^{-3} d^{-1} (Figure 7 A). There was generally higher BP in 2019 compared to 2018 and the BP peak followed the Chl-*a* maximum with highest values at 40-60 m (maximum of 0.65 mg C m^{-3} d^{-1}) at station P2, and gradually closer to the surface with decreasing distance to the ice edge, with the highest BP value measured at station P6 at 10 m (maximum of 2 mg C m^{-3} d^{-1}). The highest Chl-*a* value was measured in 2019 at station P5 at 20 m depth with 2.6 mg m^{-3}. In 2018 the highest BP was measured at the surface of station P1 with 0.4 mg C m^{-3} d^{-1}, where also Chl-*a* values were highest with 0.4 mg m^{-3}.

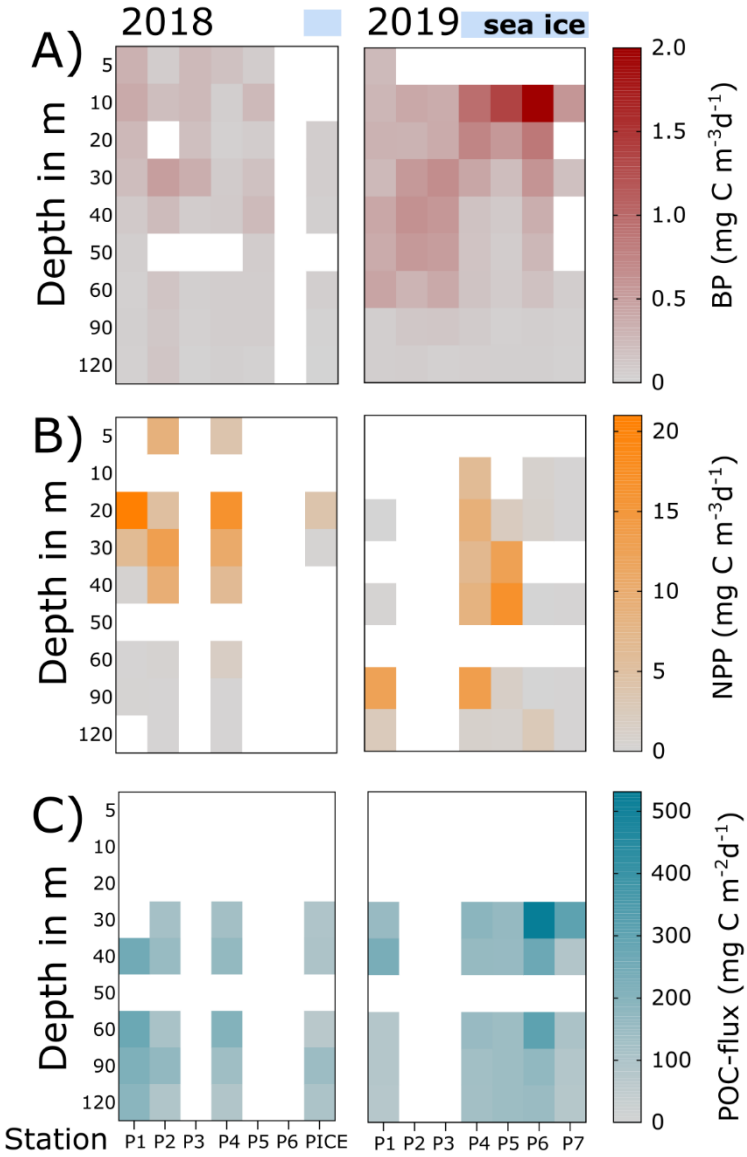

Figure 7: Heatmap of the upper 120 m of the water column for A) net primary production (NPP) in mg C m^{-3} d^{-1}, B) bacterial production (BP) in mg C m^{-3} d^{-1} and C) downward vertical flux of suspended particulate organic carbon (POC) in mg C m^{-2} d^{-1}. White background indicates that samples were not taken. The sea ice extent for the respective years is indicated with blue bars on top of the panels.

Net primary production (NPP) showed overall no significant difference (t-test, p=0.83) between 2018 and 2019 (Figure A1), but respective peaks were measured at different parts of the transect. While in 2018 NPP was highest at the surface of the southernmost station P1 with 20.8 mg C m^{-3} d^{-1}, in 2019 highest NPP was measured in subsurface samples at station P5 (16.6 mg C m^{-3} d^{-1} at 40 m). At station P1 the primary production peaks in both years followed the Chl-*a* pattern, with highest values in the surface in 2018 and at 50-60 m in 2019, but overall lower values in 2019. This was reflected in vertical POC flux (Figure 7C), which in 2018 was highest at station P1 compared to the other stations (mean of 235 mg C m^{-2} d^{-1}) throughout the upper 120 m of the water column) and around two times higher than at the same location during 2019. In 2019, POC fluxes were lowest at stations P1 and P7 (average

130 mg C m^{-2} d^{-1}) and highest at the surface of station P6 with 530 mg C m^{-2} d^{-1}. In 2019, POC fluxes were lowest at stations P1 and P7 (average 130 mg C m^{-2} d^{-1}) and highest at the surface of station P6 with 530 mg C m^{-2} d^{-1}. The northernmost stations P6 and P7 displayed a typical vertical attenuation curve, with POC fluxes between 300-530 mg C m^{-2} d^{-1} at 30 m, but decreasing to less than 30 % of that flux below 100 m. By contrast, in 2018, carbon fluxes were variable across depths but typically did not show attenuation with depth, with fluxes between 102 ± 27 mg C m^{-2} d^{-1} at Station PICE and 235 ± 43 mg C m^{-2} d^{-1} at Station P1 across all depths. Compared for the entire transect, POC fluxes were not significantly different (t-test, p=0.45) between the two years (SI Figure 1).

Elemental concentrations of particulate matter (PM)

While the concentration-range was similar for most of the elements between the years, distribution patterns were markedly different between 2018 and 2019 (Figure 8 and Figure A3). In 2018, concentrations of P, S and Ca were higher in surface waters and showed statistically significant correlations with several groups of microorganisms and Chl-*a* ($p<0.05$). In particular, calcium concentrations were significantly higher in 2018 (Welch's ANOVA: $F=4.6$, $p=0.03$). The highest concentrations were measured at the southernmost stations of the transect (P1 – P3) with highest values measured at station P1 (0.24±0.04 µM at 10 m), while in 2019 concentrations did not exceed 0.08±0.06 µM (P1 at 315 m; Figure A3). In both years bottom waters showed higher concentrations of the elements Fe, Mn, Si and O, with significant positive correlation with increasing bottom depth ($p<0.05$). However, concentrations of particulate Si were higher throughout the water column in 2019. Particulate O distribution in August 2018 and 2019 corresponded closely with that of particulate Si, which is expected as the majority of particulate O is combined with Si to form silica (SiO2) (Greenwood and Earnshaw, 2012).

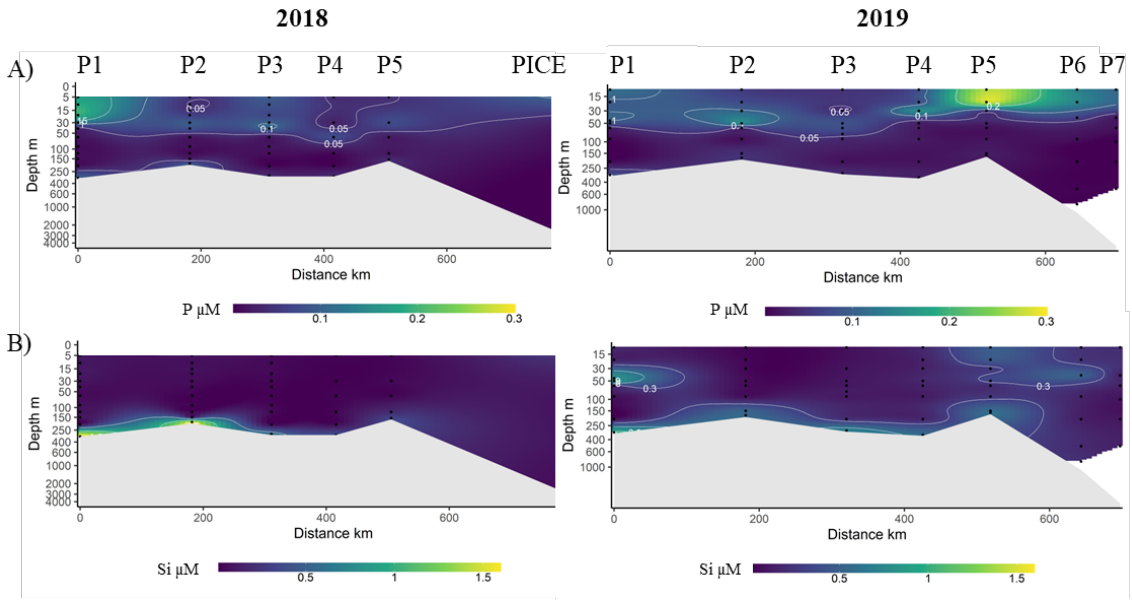

Figure 8: Elemental concentrations during August of 2018 and 2019 for all stations of the sampling transect from 76ºN to 83ºN (left to right) of A) particulate phosphorus (P) and B) particulate silicon (Si). Black dots represent sampling points and the depth axis is in log scale. Notice the different scale for each element at the bottom of each plot.

Drivers of microbial community composition and productivity

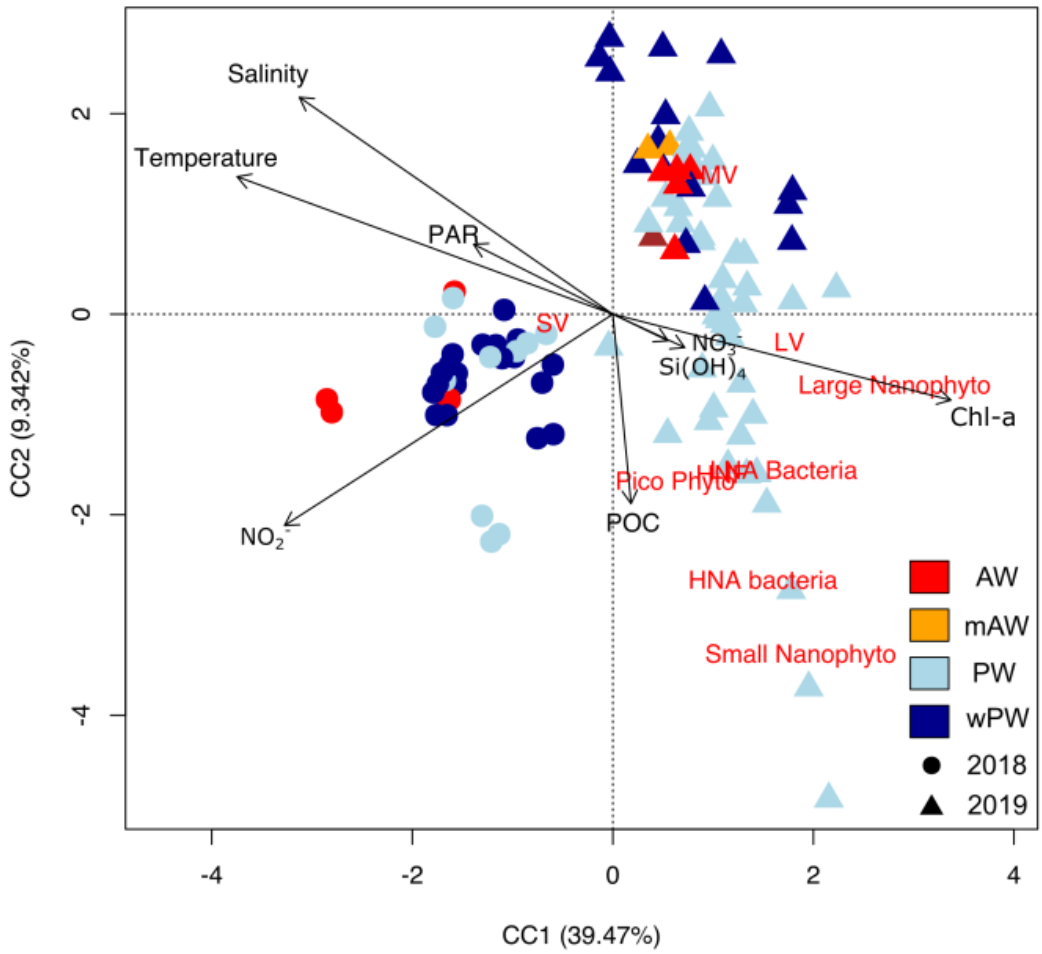

Figure 9: Visualization of the canonical correspondence analysis (CCA), using environmental variables (salinity, temperature, photosynthetically active radiation (PAR), nitrate (NO_3^-), nitrite (NO_2^-), silicic acid ($Si(OH)_4$), suspended particulate organic carbon (POC) and chlorophyll *a* (Chl-*a*)) as explanatory variables to describe variations in the microbial community composition (small virus (SV), medium virus (MV), large virus (LV), low nucleic acid containing bacteria (LNA bacteria), high nucleic acid containing bacteria (HNA bacteria), total bacteria (Bacteria), picophytoplankton (Pico Phyto), small nanophytoplankton (Small Nanophyto) and large nanophytoplankton (Large Nanophyto)).

The CCA showed a significant effect of the environmental variables on the response variables ($p<0.05$) (Figure 9). The first two axes of the CCA together explained 48.8 % of the variance in the response variables (CC1 = 39.47 %; $p<0.05$, CC2 = 9.34 %; $p<0.05$). Chl-*a*, salinity, temperature and nitrite had the strongest effects in driving the variance. Temperature, salinity and PAR were closely linked, and opposed to Chl-*a* along the first axis. Nitrite affected the samples' variance in a near-orthogonal direction from the other macronutrients, indicating a decoupling in their effects. POC was not closely related to any other explanatory variable and was only strongly correlated to the second axis.

Excluding small and medium-sized viruses, the abundance of all microbial groups was positively correlated to the first axis and negatively to the second axis. Of those, high-nucleic acid bacteria and small nanophytoplankton had the strongest influence in the ordination. The samples clustered in two distinct groups by year along CC1. 2019 was characterized by relatively higher abundances of most microbial groups, connected to increasing concentrations of Chl-*a* and POC as biomass markers. In this year, the samples were markedly spread along CC2, largely according to water mass. PW was characterized by higher abundances of all groups except medium viruses, whereas AW, mAW and wPW masses were linked to higher temperature and salinity, and lower concentrations of POC. Net primary production (NPP) was highest in PW samples with relatively low chlorophyll *a* values. In contrast, all samples grouped closely together in 2018 and abundances of most microbial groups were lower, except for small viruses. Samples from 2018 were defined by higher temperature, salinity and nitrite, and lower values of Chl-*a*.

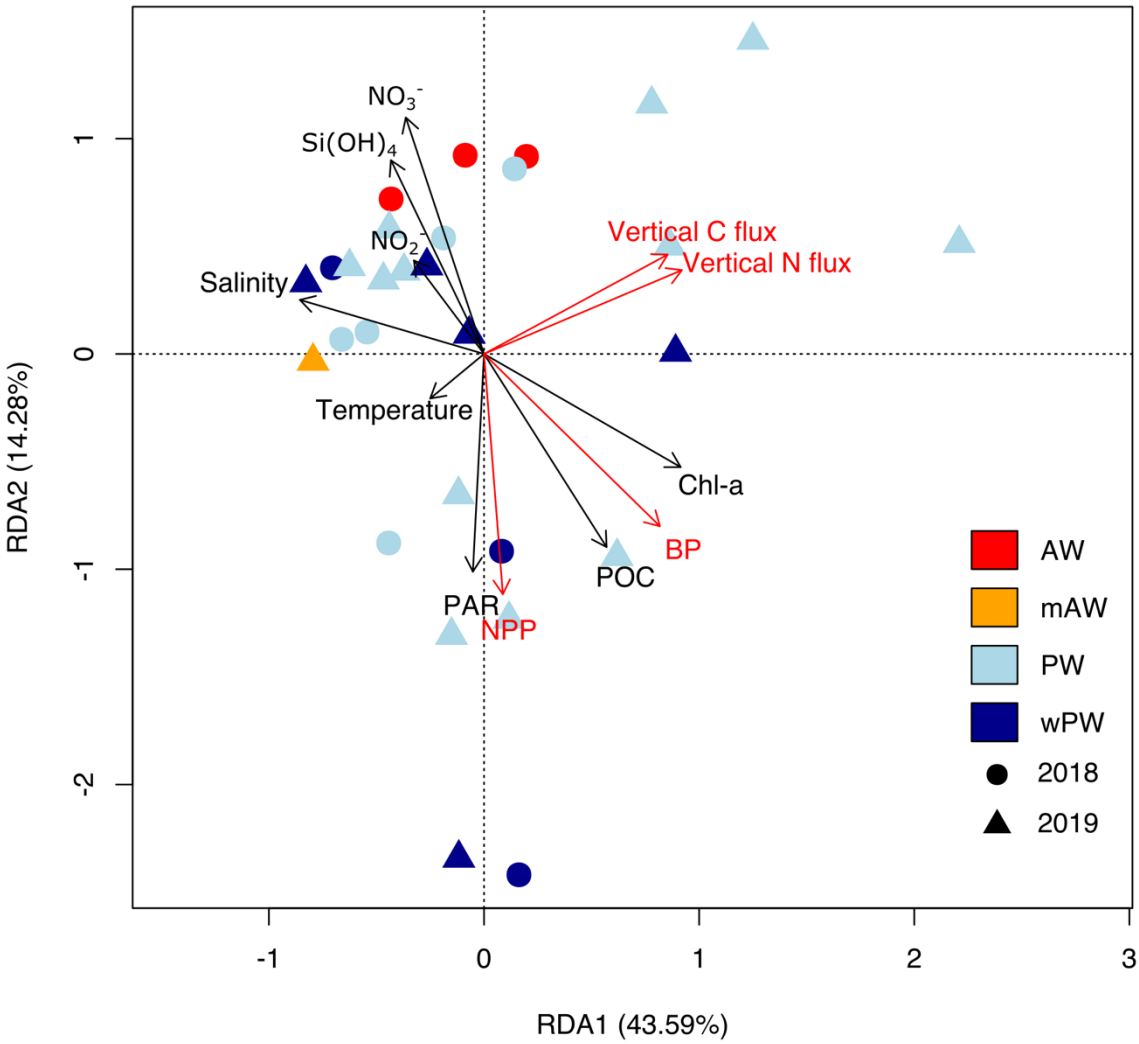

Figure 10: Visualization of the redundancy analysis (RDA) showing effects of environmental variables (salinity, temperature, photosynthetically active radiation (PAR), nitrate (NO_3^-), nitrite (NO_2^-), silicic acid ($Si(OH)_4$), suspended particulate organic nitrogen (PON) and chlorophyll *a* (Chl-*a*)) on the variation of net primary production (NPP), bacterial production (BP), vertical POC/PON flux.

The RDA revealed a significant effect of the selected environmental variables on the studied carbon flux variables ($p<0.05$). The first two axes of the RDA explained a total of 57.87 % of the variance of the response variables (Figure 10). Axis RDA1 explained 43.59 % of the total variance ($p<0.05$), and axis RDA2 explained 14.28 % of it ($p<0.05$). Chl-*a*, POC, PAR, nitrate, silicic acid and salinity had similarly strong effects in driving the variance. Temperature and nitrite had the lowest relative effect in this ordination space.

NPP was most strongly positively linked to increasing levels of PAR and lower levels of all macronutrients. BP was positively correlated to biomass indicators POC and Chl-*a*, and partially to lower levels of macronutrients. Vertical POC/PON fluxes were relatively higher in colder, fresher waters and partially associated with higher Chl-*a* concentrations.

All three response variables contributed similarly to the ordination. NPP and vertical flux were not closely related to each other, while BP was more closely linked to NPP than to vertical flux. Vertical flux was most associated with high concentrations of Chl-*a*, as well as lower temperature and salinity. Sample distribution did not reveal any clear grouping by year or water mass. Nonetheless, 2019 samples showed a greater spread along RDA2, driven by high vertical flux values in PW samples.

For each of the carbon flux parameters, the simplest model that retained the most information is shown in Table 1.

Table 1: Multiple regression models assessing the effects of environmental drivers on carbon flux variables, as selected by a stepwise algorithm based on AIC. Asterisks indicate a significant effect.

Variable	Terms	AIC	R^2
Net primary production (NPP)	$-201.56 - 0.52 \times [NO_3^-]^* + 57.45 \times \text{salinity} - 0.53 \times \text{temperature} + 0.18 \times \text{Chl-}a$	78.33	0.45
Bacterial production (BP)	$12.76 - 0.06 \times [Si(OH)_4^-]^* + 0.08 \times \text{POC} - 3.57 \times \text{salinity} + 0.06 \times \text{temperature}^* - 0.08 \times \text{PAR}^* + 0.04 \times \text{Chl-}a^*$	-61.73	0.75
Vertical carbon flux	$116.49 - 0.19 \times [Si(OH)_4^-]^* - 31.19 \times \text{salinity}^* + 0.17 \times \text{temperature} - 0.42 \times \text{PAR}^*$	29.18	0.39

Discussion

Earlier sea ice retreat altered mixing, nutrient and light regimes

The sampling transect following a latitudinal gradient from 76ºN to 83ºN in the north-western Barents Sea allowed for the investigation of environmental variability in water masses, ice cover and associated effects on the MMFW. The observed ice conditions in August 2018 and 2019 were a response to oceanographic and meteorological conditions during the previous months (Figure 1), including heat transported via the Atlantic water inflow (Årthun et al., 2012). The two sampling years are conspicuous examples of contrasting summer situations in the north-western Barents Sea, with comparatively low versus high sea-ice concentrations as the main driver of the observed differences (Ingvaldsen et al., 2021; Rieke et al., 2022). With the transect being ice-free in late summer of 2018 and mainly ice-covered in 2019 (Figure 1), the two years are further glimpses into the future and the past of the Barents Sea ecosystem, respectively.

Differences in the water mass distribution between the two years resulted from the aforementioned processes. The dominance of wPW in 2018 was likely a result of the earlier retreat of sea ice that exposed the surface PW to atmospheric warming for a longer time. The stronger inflow of AW compared to 2019 led to more mixing with PW in the southern Barents Sea stations, further modifying it (Figure 2 and 3). Less melting sea ice and related less freshwater input weakened the vertical stratification (Lind et al., 2018). Additionally, the AW likely provided more heat and salinity to the mixed layer depth as it was much closer to the surface in 2018 (ca. 30 m depth) compared to 2019 (ca. 70 m). In 2019, nutrient regimes followed a latitudinal pattern, with maximum nitrate concentrations found at greater depths with increasing distance to the ice edge (Figure 4c). This is consistent with known theories of phytoplankton nutrient consumption and deep chlorophyll *a* maxima in late summer (Carmack and Wassmann, 2006; Hill and Cota, 2005). Accordingly, for most of the 2018 transect microbial productivity was more nutrient limited since phytoplankton bloom onset happened earlier in that year (Kohlbach et al., 2023). This pattern was broken at station P1 due to the shallower AW presence, which raised the nutricline to 25-60 m, compared to 50-90 m at station P2. Less sea ice also increased irradiance and euphotic zone depth in 2018 compared to 2019. Furthermore, the difference between the shallowest and deepest euphotic depth in 2018 was smaller, showing similar steep gradients in light as in stratification regimes and nutrients in 2019 (Table A2).

Overall, the PCA showed distinct environmental assemblages in the high-ice and low-ice years. The PW in 2019 was divergent from any other group in terms of relative contribution of environmental drivers. In 2018, wPW clustered distinctly into two groups, a surface group linked to lower nutrient concentration and higher biomass, and a deeper cluster more closely influenced by AW, which resulted in higher nutrient concentrations and lower biomass. In 2019, however, the wPW samples were more evenly spread out between the two extremes. In all, the 2019 transect was more latitudinally structured than in 2018, in which the main

differences in environmental parameters were driven by the strong inflow of AW in the southern Barents Sea.

Sea ice structured the microbial community composition along a latitudinal gradient

Distinct differences in biological variables between 2018 and 2019 were related to the hydrographical patterns. Generally, phytoplankton biomass, estimated as Chl-*a*, nanophytoplankton abundance (especially large nanophytoplankton) and bacterial abundance (all size groups) were higher in 2019, while the abundance of picophytoplankton and HNF was higher in 2018. The higher abundances of larger nanophytoplankton and bacteria in 2019 were mainly associated with the layer of colder and relatively fresher PW that could form due to the presence of sea ice in spring that melted throughout the summer (Figure 1 and 3). The size difference in primary producers based on flow cytometry is also supported by microscopical analyses, which showed for 2019 that diatoms were important phytoplankton biomass contributors in the upper water column, especially at the ice-covered stations (Kohlbach et al., 2023). The species assemblage at these stations was dominated by oceanic diatom species of the genera *Fragilariopsis, Chaetoceros* and *Rhizosolenia* (Kohlbach et al., 2023), which often occur in MIZ associated phytoplankton blooms in the Barents Sea (Signorini and McClain, 2009; Wassmann et al., 1999). Relatively high Chl-*a* concentrations of up to 2.6 mg m^{-3} and high nanophytoplankton abundances of up to 3000 cells mL^{-1}, as well as high abundance of larger phytoplankton (>20 µm; Kohlbach et al., 2023) at the ice edge stations denote that we sampled the remnants of an ice-edge associated bloom during August 2019, as Chl-*a* concentrations can reach up to 20 mg m^{-3} during bloom conditions earlier in the season (Engelsen et al., 2002). Consequently, the stations located south of the ice edge in 2019 were in successively later stages of this post-bloom scenario. This is supported by the subsurface Chl-*a* maxima, nanophytoplankton abundances, NPP and BP, as well as the nutriclines, which all shifted progressively deeper with distance to the ice edge due to persistent nutrient drawdown by phytoplankton exacerbated by persistent stratification in the stations along the continental shelf (Strass and Nöthig, 1996). Accordingly, the standing stocks were dominated by flagellates, dinoflagellates and ciliates (Kohlbach et al., 2023), as is described for this time of the year, when meltwater driven stratification has enabled nutrient drawdown by phytoplankton during an extended period of time (Rat'kova and Wassmann, 2002a; Sakshaug et al., 1991). Another possible explanation for the observed latitudinal differences in abundance for some phytoplankton groups in 2019 could be attributed to virus activity, which has been recently highlighted as important factor for Antarctic phytoplankton (Eich et al., 2022) and specifically diatoms (Kranzler et al., 2019). This is indicated by high concentrations of large viruses and simultaneously low abundance of large nanophytoplankton in the upper 20 m of the water column, highlighting a possible virus control on the nanoplankton community at an earlier time point (Figures A5 and A8).

With sea ice being mostly absent during August 2018, such an ice melt related latitudinal gradient was not observed at the time of sampling. In August 2018, overall biomass and abundance of microorganisms were lower compared to 2019. Chl-*a* concentrations were highest in the surface of station P1 (0.4 mg m^{-3}) and below 0.3 mg m^{-3} for the rest of the transect. These low Chl-*a* concentrations are typical for late summer conditions in the Barents Sea and a result of nutrient depletion (Dalpadado et al., 2014; Sakshaug et al., 2009), as seen

by the low nutrient concentrations in surface waters in August 2018 (Figure 4). This late summer condition with low biomass and low production is further evident in the composition of the microbial community, with relatively high concentrations of picophytoplankton and HNF (Figure 5), which are thriving in nutrient limited environments (Litchman et al., 2007; Zhang et al., 2016). Arguably, the longer exposure to open water in 2018 and subsequent later stage of seasonal succession uniformized the transect, with the MMFW community converging to similar compositions regardless of water mass and depth, as evidenced by the CCA (Figure 9). Instead of a MIZ driven gradient, nutrient concentrations and ultimately AW inflow were the strong drivers for community composition as well as primary and bacterial production (Figure 9 and 10).

The observed subsurface maximum of Chl-*a*, NPP and BP at P1 in 2019 coincided with high particulate Si concentrations, related to the higher diatom contributions (Kohlbach et al., 2023) (Figure 8). Similar concentrations of particulate Si were found near the surface at the MIZ station, strengthening the picture of a post-bloom stage ecosystem. Diatoms are typically found dominating at the start of the phytoplankton community succession, outcompeting other algal groups in uptake of nutrients like NO_3^- and PO_4^{3-} (Assmy et al., 2023; Egge and Aksnes, 1992; Larsen et al., 2015; Thingstad et al., 2005), while dissolved Si is available in the euphotic zone in sufficient concentrations. Increased concentrations of particulate Si were found in bottom waters throughout the transect in 2019, and at stations P1 and P2 in 2018. The increased concentrations of Si at these depths, together with increased concentrations of other elements such as iron, suggests the presence of resuspended sediments. A survey carried out in the Nansen Basin during the same period as this study measured large scale transport into the basin of particles suspended in bottom water, which were traced back to their source in the Barents Sea shelf (Rogge et al., 2022). It is likely that the particles observed in our study are part of this lateral transport and contribute to the storage of carbon in the deep Arctic Ocean.

Calcium is particularly important for calcifying planktonic organisms, as it is a basic component of their cell wall structures in the form of calcium carbonate ($CaCO_3$). *Emiliania huxleyi*, a marine coccolithophore, is one of the most important marine $CaCO_3$ producers (Fagerbakke et al., 2012; Krumhardt et al., 2017; Langer, 2008), and is particularly abundant in the North Atlantic (Krumhardt et al., 2017). This species has in recent years increased in importance in the Barents Sea and thus been described as a putative indicator of a changing Arctic (Hegseth and Sundfjord, 2008; Orkney et al., 2020; Oziel et al., 2020). Concentrations of elemental Ca were much lower in the northern parts of our sampling transect in both 2018 and 2019 (Figure A4). In the southern Barents Sea, the concentration of particulate Ca was up to an order of magnitude higher in 2018. Furthermore, only at station P1 in 2018 low abundance of *Emiliania huxleyi* was detected (Kohlbach et al., 2023). This supports the concept of AW transporting organisms into the Arctic via the Barents Sea, and how the differences in AW inflow between 2018 and 2019 influenced the community composition.

Contrasting nutrient sources maintained comparable regimes of carbon production and export

Despite the described contrast in environmental setting, microbial community composition and bacterial production, no significant differences were found in the magnitude of NPP and POC/PON export below 100 m (Figure A1). This was further supported by our redundancy analysis, which showed no clear sample groupings based on year or water mass beyond an overall larger spread in 2019.

Although the overall ranges overlapped, the distributions of NPP, BP and POC/PON fluxes in latitude and depth were starkly different in both years. In 2019, maximum values of NPP were detected near the surface at the stations closest to the ice edge (chiefly P5). Further south in the transect, peaks of NPP shifted deeper into the water column, reaching a maximum depth at the southernmost station (P1). This north-to-south progression of the MIZ bloom is an extensively described phenomenon in the central Barents Sea (Sakshaug et al., 1991; Wassmann, 2002a). The elemental concentrations of phosphorus as a proxy of biological activity further support this interpretation (Arrigo, 2004; Erga et al., 2017), as they were highest near the surface at P5, and were overall lower and found at greater depths in the rest of the transect. Surface pelagic NPP in our ice-covered stations, which ranged from 0.6 to 3.88 mg C m^{-3} d^{-1}, was lower than other surveys done in the northern Barents Sea in late July (13-14 mg C m^{-3} d^{-1}, (Nøst Hegseth, 1998)), but comparable to other estimates performed in the Central Arctic Ocean basins in summer (0.2 mg C m^{-3} d^{-1}, (Hill and Cota, 2005)). Pelagic NPP in this study's MIZ stations was well within range (0.6 to 16 mg C m^{-3} d^{-1}) of other late summer studies in the area (0-12 mg C m^{-3} d^{-1}, (Eilertsen et al., 1989)), which also showed maximum values of NPP at depths ranging from 20 to 40 m.

In 2018, contrastingly, MIZ-associated algal growth was not detected during our sampling time, and no clear latitudinal gradient in NPP linked to the MIZ was observed, likely due to the earlier onset of the sea ice melt. In a 21-year analysis of the phytoplankton bloom phenology of the Barents Sea, Silva et al. (Silva et al., 2021)) found that spring bloom intensity in the area was negatively correlated with its onset, duration, and peak day, implying that when the spring bloom is earlier, it is also shorter and more intense. Such a short, strong bloom corresponds with the regimes of nutrients, NPP and Chl-*a* described above. A notable exception to this pattern was station P1, which contained the highest levels of NPP in the transect. Accordingly, previous studies in the area have reported very similar daily NPP estimates in open water during August (20.8 mg C m^{-3} d^{-1} at 20 m this study, 22 mg C m^{-3} d^{-1} (Nøst Hegseth, 1998)). High concentrations of elemental phosphorus but low concentrations of elemental Si at station P1 in 2018 indicate that the active fraction of phytoplankton was not dominated by diatoms, even though they contributed a significant fraction to total protist biomass at this location (Kohlbach et al., 2023). Concentrations of nitrate and silicic acid were higher than in 2019 in the uppermost 60 m of the water column. The presence of these nutrients and associated algal growth can be explained by the different water mass distribution in the two years. In 2018, station P1 was dominated by Atlantic and modified Atlantic Water, whereas in 2019 it was predominantly occupied by warm Polar Water. This Atlantic Water inflow penetrated further into the Barents Sea in 2018, and advected both nutrients and microbial organisms from the North Atlantic. Interestingly, a similar study in the Laptev Sea comparing two years with contrasting sea-ice cover showed overall higher primary

production in the year with less sea-ice, but with a high spatial variability and associated with rapid nutrient-limitations (Bienhold et al., 2022). The role of advection and autumn vertical mixing in the development of autumn blooms in the southern Barents Sea is known, but not yet thoroughly studied (Orkney et al., 2022; Oziel et al., 2017). In the RDA, NPP was most closely related to light and nutrients, known drivers of algal physiology (Sverdrup, 1953). In the fitted generalized linear model, only nitrate concentrations were proven to be significantly linked to NPP variation, further exemplifying the importance of advected nutrients in the areas of the Barents Sea affected by AW inflow.

Bacterial production followed a similar pattern in space. In 2019, BP was highest closer to the surface in the MIZ, and deeper further south. In 2018, the transect was uniformly lower in BP, with a less marked vertical structure. Bacterial production rates measured during both cruises ranged between 0.01 to 2.0 mg C m^{-3} d^{-1}, which is within the range of measurements which were done in the same area in July and August (<0.05 to 2.8 mg C m^{-3} d^{-1}, (Howard-Jones et al., 2002a) and 0.1 to 0.8 mg C m^{-3} d^{-1}, (Piontek et al., 2021)), but lower when a slightly different method was applied (5.6±5.3 mg C m^{-3} d^{-1}, (Sturluson et al., 2008)). Our measured rates are further within the range of what has previously been reported for other Arctic areas (0.02–1.5 mg C m^{-3} d^{-1}), with higher values associated to bloom phases and lower values to pre-bloom conditions (Cota et al., 1996; Kirchman et al., 2009b; Piontek et al., 2021; Rich et al., 1997; Steward et al., 1996; Uchimiya et al., 2016). In our multivariate analysis, BP was highly correlated with biomass markers POC and Chl-*a* rather than with NPP. This is likely due to the delay between NPP onset, accumulation of biomass and utilization of organic matter by bacteria, which is exacerbated in colder waters (Pomeroy et al., 1991). In fitting a linear model, the variables that were found to significantly affect BP were $Si[OH]_4^-$, PAR, Chl-*a*, and temperature, which reflect the link from bottom-up drivers to microbial metabolism.

Station P6 in 2019 is worth noting. For most of the transect, the total abundance of bacteria closely matched the high nanoplankton abundance. However, the highest levels of BP were measured at the surface of station P6, where total bacterial abundance was an order of magnitude lower. Interestingly, at station P6, the ratio of HNA, the large and active fraction of the bacterial community to total bacteria counts, was highest. A high correlation for HNA and bacterial activity has previously been shown when bacteria were likely controlled by substrates from phytoplankton (Moran et al., 2007) and metabarcoding analyses showed a high dominance (>60 %) of the genus Polaribacter (Thiele et al., this special issue). This is to some extent also likely for the HNA bacteria at station P6 in 2019, not necessarily by fresh substrates from growing phytoplankton, but rather material released from the ice. This is further supported by low pelagic primary production, but high vertical flux measurements at 30 m depth. High abundance of HNA-bacteria in sea ice has been reported before and correlated with Chl-*a* and sea ice temperature (Ugalde et al., 2014). During the first phases of sea ice melt, the sea ice gets flushed and releases organic material, nutrients, and the organisms inhabiting the sea ice (Eicken, 2003; Hudier and Ingram, 1994) into the water column below. Moreover, HNF concentrations in the uppermost 20 m at this station were two orders of magnitude higher than those found below the mixed layer depth. This probably indicates predation of HNF over the aforementioned active bacteria and a tightly coupled microbial food web, as observed in other seasonally stratified Arctic waters in late summer (Iversen and Seuthe, 2011).

In the study area, vertical carbon fluxes are known to be highly variable throughout space, seasons, and years (Wassmann et al., 2004). While vertical flux is generally correlated to high levels of new (supported by inorganic nutrients entrained in the water column through winter mixing) NPP, there are several factors that control the efficiency of this export, such as the mixed layer depth, the phytoplankton community composition, and/or the grazing efficiency by predators (Carmack and Wassmann, 2006; Wiedmann et al., 2020). Previous studies in the area have found that in a post-bloom stage, daily vertical flux rates measured with short-term sediment traps in the uppermost 200 m ranged between 110 and 230 mg C m^{-2} d^{-1} (Reigstad et al., 2008) and 108-215 mg C m^{-2} d^{-1} (Dybwad et al., 2021), all within range of our measured fluxes (90-270 mg C m^{-2} d^{-1}) excluding the MIZ stations in 2019. Daily vertical flux ranges at the MIZ stations in this study (63-398 mg C m^{-2} d^{-1}) were lower compared to "peak bloom" stations in the aforementioned studies (120-870 mg C m^{-2} d^{-1} in (Reigstad et al., 2008); 150-513 mg C m^{-2} d^{-1} in (Dybwad et al., 2021)), conforming with Chl-*a* concentrations that indicated that the peak had passed at the time of this survey.

It is worth noting that in previous studies in "spring bloom" scenarios, a very strong attenuation signal was detected in vertical flux, with export production at 100 m reaching 17 % of the flux nearest to the surface in extreme cases (Dybwad et al., 2021). Similarly for this study, POC/PON fluxes were particularly high in the surface PW masses of the northernmost stations P6 and P7 in 2019 and showed a very sharp decline with increasing depth. While vertical carbon fluxes at 30 m were higher in 2019, particularly in the MIZ, export fluxes below 90 m were comparable across the transect between the two years. Typically, vertical flux is attenuated with depth, because sinking organic material is remineralized by grazing and microbial degradation within the water column (Iversen, 2023; Martin et al., 1987). Akin to BP and NPP, high vertical flux was also found to be associated with the MIZ in 2019; displaying a strong attenuation curve, while no attenuation of vertical flux was present in 2018. Vertical flux attenuation in the Arctic is strengthened by meltwater stratification, since the pycnocline provides a physical barrier which constrains vertical export and ultimately can sustain longer-duration blooms (von Appen et al., 2021). In the northern Barents Sea, attenuation has indeed been shown to be lower in late summer or post-bloom situations compared to peak bloom scenarios (Dybwad et al., 2021; Reigstad et al., 2008), further indicating that the 2018 transect was at a later stage of the ecological succession.

These contrasting attenuation regimes might also point towards a more efficient pelagic retention system in 2019, which would be supported by the overall higher BP. Vertical flux to the sea-floor in a study conducted in the Laptev Sea in two years with different sea ice cover was also comparable between the years and similar to our study, even though during the year with larger sea-ice extent, the authors suspected higher surface production but stronger pelagic recycling (Bienhold et al., 2022). This meltwater effect is supported in the RDA of this study, in which POC/PON fluxes are very strongly correlated to lower values of temperature and salinity. Indeed, the effect of salinity in the fitted linear model was two orders of magnitude higher than that of the rest of explanatory variables. Interestingly, the above patterns of vertical carbon flux were detected in ice covered stations with low to non-detectable pelagic NPP. Given the corresponding high levels of BP at the same locations, it is possible that this high surface vertical flux is being driven by sea ice algal growth and export. Indeed, the sea ice algal biomarker IP_{25} was only detected in the sediment traps at station P6 (Yasemin Bodur Unpubl. Data).

The Barents Sea ice cover shows strong interannual variability, in addition to the observed long-term downward trend over the last decades (Yamagami et al., 2022). Our two observational periods lay clearly above (August 2019) or below (August 2018) this trend line. The maximum March sea ice extent in 2019 exceeded all previous years since 2004 (EUMETSAT, 2023) and the highest values for August/September in the period 2015 to 2022. Oppositely, 2018 was the year with the lowest August sea ice extent on record in the Barents Sea (EUMETSAT, 2023) and substantially below the long term trend line. When contrasting our observations to data from previous years, both the interannual variability and the long-term trend need to be considered, having shifted the scale on what is considered a low versus a high ice year. The lack of consistent long-term time series, partially due to the logistical challenges of sampling in Arctic marine waters, complicates a framework of understanding the ecological impacts of interannual variability of ice cover on the marine ecosystem. We selected two previous summer field expeditions that we considered as high ice year (July 1999, (Wassmann, 2002b)) and low ice year (August 2011, (Wiedmann et al., 2014)).

In July 1999, the average sea ice extent was 0.35 Mkm^2, exceeding this study's "high ice" year, 2019 (0.17 Mkm^2 average sea ice extent in August). Similarly to our data, a strong latitudinal gradient in bloom phenology was reported, with the diatom dominated stations closest to the MIZ experiencing incipient nitrate limitation and progressing towards post-bloom conditions further south, dominated by small flagellates (Verity et al., 2002,Rat'kova and Wassmann, 2002b). Also akin to our data, maximum pelagic NPP was found in the surface of the open water stations closest to the MIZ (Matrai et al., 2007), combined with highest pelagic BP and vertical POC/PON fluxes (Howard-Jones et al., 2002; Olli et al., 2002).

The summer of 2011 experienced very low ice conditions with an average August sea ice extent of 0.02 Mkm^2, comparable to the 0.01 Mkm^2 found in August 2018. A study conducted in late June of 2011 reported vertical fluxes concordant with a "late-peak bloom" stage in the central Barents Sea, shifting towards "late bloom" and "post bloom" stages in stations further south (Wiedmann et al., 2014). This high-flux, latitudinally structured system in June likely shifted into a low-flux, low-production uniform transect as the summer progressed, similar to our August 2018 data.

Further evidence of this phenological shift was provided by Downes (2022), as part of a survey in the same area as this study but in July of 2018 and 2019. Interestingly, the observations in July 2018, were nearly identical to our August 2019 data. Subsurface maxima of NPP and BP were found at 20-40 m depth, highest nearest to the ice edge, and overall estimates were well within range of those described here. The consistently high July 2019 pelagic NPP values at the surface throughout most of the transect indicated that the pelagic NPP was not yet controlled by nutrient depletion (Downes, 2022). Interestingly, the distinctly high NPP/BP values found at station P1 in 2018 in this study were already observable in comparable magnitude in July, weeks before this study's sampling. This indicates either a persistence or a reoccurrence of the advection-driven growth in the Atlantic-dominated Southern Barents Sea in late summer proposed above and warrants further investigation.

Summary

This study showed that differences in sea ice phenology and Atlantic water inflow had a drastic impact on community composition in the late summer Barents Sea, by changing access to light and nutrients, as well as water mass distributions. Contrastingly, statistical analysis did not show significant differences in primary production or vertical flux between 2018 and 2019. The relationship between carbon flux variables and physical drivers was consistent with previous findings and persistent throughout both years. Nonetheless, the peaks of production and vertical export were located at opposite ends of the transect in both years and were originated by ecologically diverse phenomena. In a cold, high-ice year, late summer production was concentrated in the MIZ, where access to light and nutrients by a diatom-dominated community was regulated by sea ice melt. In a warm, low-ice year, maximum growth by small pico- and nano-flagellated cells was located at the southernmost station and sustained by less stratified Atlantic water. This is further reflected in the different Chl-*a* concentrations that we measured. The smaller cells, dominant in 2018, were exposed to higher light conditions and had less Chl-*a* than the larger cells in 2019 that were adapted to lower light conditions under the ice. Even though Chl-*a* was significantly higher in 2019, measurements of primary production were comparable in both years, potentially due to differences in grazing pressure or low light adaptations. This is a critical factor that should be considered when modelling NPP based on Chl-*a* concentration. Further, while the phenomenon of autumn blooms might provide an influx of organic carbon in the southern Barents Sea MMFW in low-ice years, it remains to be seen whether it can compensate for extended periods of nutrient limitation in the northern Barents Sea and what the fate of this carbon is in terms of availability to different consumer groups as well as pelagic-benthic coupling.

Data availability statement

Chlorophyll *a* (Vader, 2022), nutrient (Chierici et al., 2021a,b), elemental composition of particles (Tsagkaraki et al., 2023), bacterial production (Müller et al., 2023a), flow cytometry (Müller et al., 2023b) and CTD (Ingvaldsen, 2022; Reigstad, 2022) data have been published in the Norwegian Marine Data Centre. Phytoplankton biodiversity data (Assmy et al., 2022a,b) have been published in the Norwegian Polar Data Centre and GBIF. Suspended POC/PON and vertical downward flux of POC/PON data have been published in the National Infrastructure for Research Data (NIRD; Marquardt et al., 2022; Bodur et al., 2023a, b).

Funding

This work was funded by the Research Council of Norway through the project The Nansen Legacy (RCN # 276730).

Author Contributions

MA and OM contributed equally to the writing of the initial draft, as well as data analysis and interpretation and preparation of figures. YB, IN, TV, PA, DK, MC, EJ, LO, TT, MR, GB, RG were all involved in data interpretation and revising the draft as well as providing ideas for improvement. Initial project development and conceptualization was supported by MC, PA, GB, RG and MR. Nutrient data were analysed by MC and EJ. MA and TV contributed to primary production data, OM, GB and LO contributed to flow cytometry data and bacterial production data. Flow cytometry data was contributed by TT and IN. Vertical flux data was contributed by YB and MR. All authors contributed to data interpretation and to the writing of the manuscript.

Declaration of Competing Interest

The authors declare that they have no known competing financial interests or personal relationships that could have appeared to influence the work reported in this paper.

Acknowledgments

The authors would like to thank the captain and the crew of Kronprins Haakon for their excellent support at sea during the Nansen Legacy expeditions in 2018 (JC1-2) and 2019 (Q3). We thank Miriam Marquardt (UiT) for support and help during the field sampling in 2019. We thank Paul Dubourg (UiT) for his help in analysing the POC samples. We thank Evy Foss Skjoldal (UiB) for taking flow cytometry samples during the 2018 expedition and Elzbieta Anna Petelenz (UiB) for laboratory analysis of flow cytometry samples. We thank Raul Primicerio (UiT) for his guidance on multivariate statistics methods. We thank Frida Cnossen (UiT) for the elaboration of the graphical abstract.

Appendix

Table A1: Depth-integrated (0-120 m) values for each process stations during the cruises in August 2018 and 2019 for following parameters: chlorophyll *a* (chl-*a*); suspended particulate organic matter (POC); vertical flux of POC; primary production (NPP), bacterial production (BP); and abundance of different microbial groups.

Cruise	August-2018						August-2019						
Station	P1	P2	P3	P4	P5	PICE	P1	P2	P3	P4	P5	P6	P7
Chl-*a* (mg m^{-2})	9.8	12.6	7.2	3.3	9.0	5.8	34.2	51.2	48.0	45.5	69.4	49.5	51.0
POC (g m^{-2})	15.9	14.7	8.9	10.8	9.0	10.4	10.2	12.7	14.4	12.0	10.6	10.7	8.2
vertical flux POC (g m^{-2} d^{-1})	29.1	15.7	nd	17.5	nd	12.4	14.6	nd	nd	18.6	17.9	37.7	18.4
NPP (g m^{-2} d^{-1})	1.0	0.5	nd	0.8	nd	0.0	0.3	nd	nd	1.4	0.8	0.7	-0.2
BP (mg m^{-2} d^{-1})	13.7	24.4	12.5	7.1	12.5	4.5	28.7	37.2	39.5	32.3	33.2	56.3	19.5
Picophytoplankton (x 1000 cells m^{-2})	55.0	150	219	438	370	242	72.4	102	271	288	156	27	106
Nanophytoplankton (x 1000 cells m^{-2})	64.0	21.5	31.0	28.8	9.4	29.7	44.2	110	87.0	134	89.3	32.7	93.3
HNF (x 10^3 cells m^{-2})	33.1	43.0	70.7	92.0	23.9	21.8	15.3	47.8	38.7	46.4	28.4	37.4	26.9
Bacteria (x 10^6 cells m^{-2})	31.8	30.1	36.9	31.5	47.5	36.3	28.1	80.1	95.8	70.6	76.1	34.9	41.6
LNA bacteria (x 10^6 cells m^{-2})	6.6	7.2	12.3	10.9	9.4	10.9	7.9	31.9	32.8	26.3	21.8	8.1	13.3
HNA bacteria (x 10^6 cells m^{-2})	23.8	22.0	23.5	19.4	36.5	23.5	19.2	47.1	61.5	42.9	52.8	23.2	27.3

Table A2: Measured or estimated (*) surface irradiance, ice concentration and calculated euphotic zone depth for each of the stations during the cruises in august 2018 and 2019.

Cruise	August-2018						August-2019						
Station	P1	P2	P3	P4	P5	PICE	P1	P2	P3	P4	P5	P6	P7
Surface irradiance (µmol photons m^{-2} s^{-1})	5.7	91.9	50.9	107.9	66.3	5.8*	46.3	15.4*	37.4*	73.5*	59.1*	10.8*	52.1*
Ice concentration (%)	0	0	0	0	0	80	0	0	0	60	80	90	90
Euphotic zone depth (m)	158	89	95	89	83	68	76	83	63	41	61	84	15

1

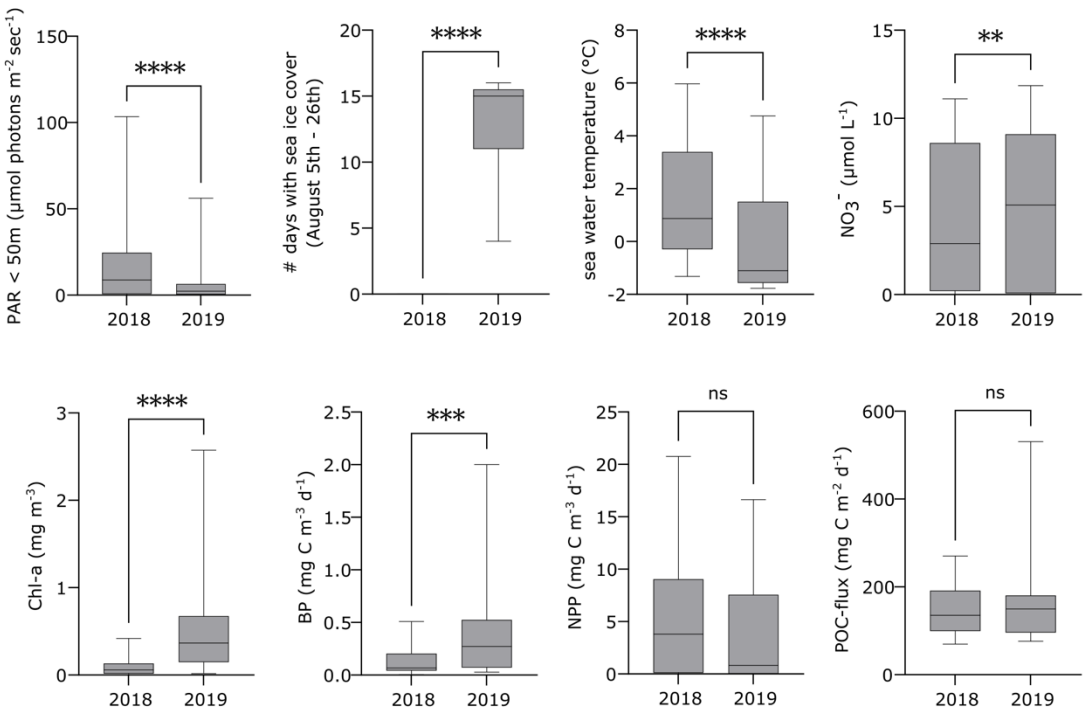

2

Figure A1: Boxplots of photosynthetically active radiation (PAR) (n=248), number of days with sea ice cover between station P1 to P7 during the period August 5th to 26th (n=21), sea water temperature (n=47), nitrate (NO_3^-) (n=45), chlorophyll *a* (Chl-*a*) (n=42), net primary production (NPP) (n=10), bacterial production (BP) (n=38) and suspended particulate organic carbon flux (POC-flux) (n=14) comparing all measured values of the upper 120 m (PAR upper 50 m) between 2018 and 2019. Statistical significance (paired t-test) is indicated by the asterisk ($p<0.0001$:****; $p<0.001$:***; $p<0.01$:**; ns=no significance difference between the two years).

3

4

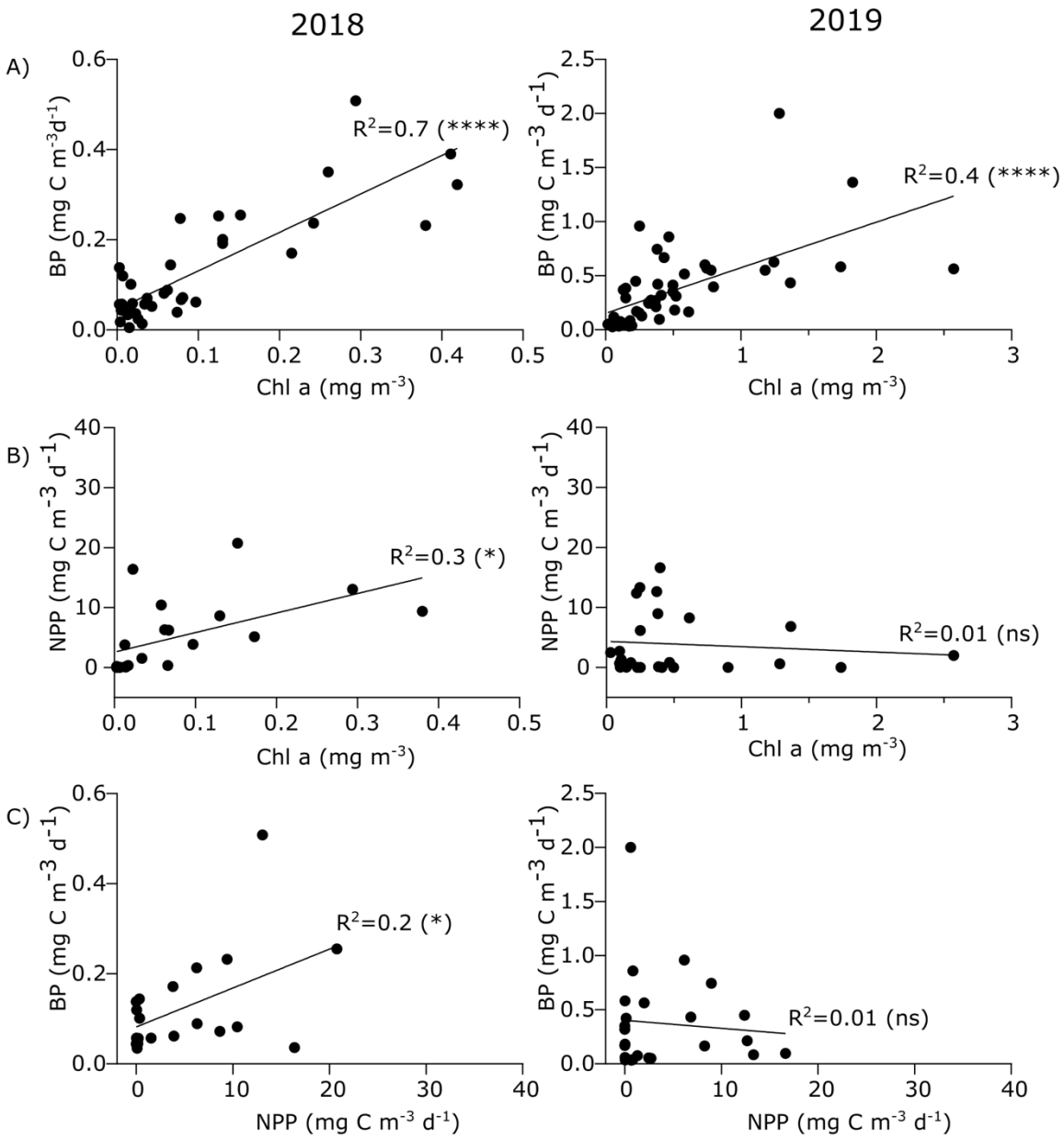

1

Figure A2: Linear regression analyses for each 2018 (left) and 2019 (right) of A) bacterial production (BP) against chlorophyll *a* (Chl-*a*) concentrations, B) net primary production (NPP) against Chl-*a* concentrations and C) BP against NPP.

2

3

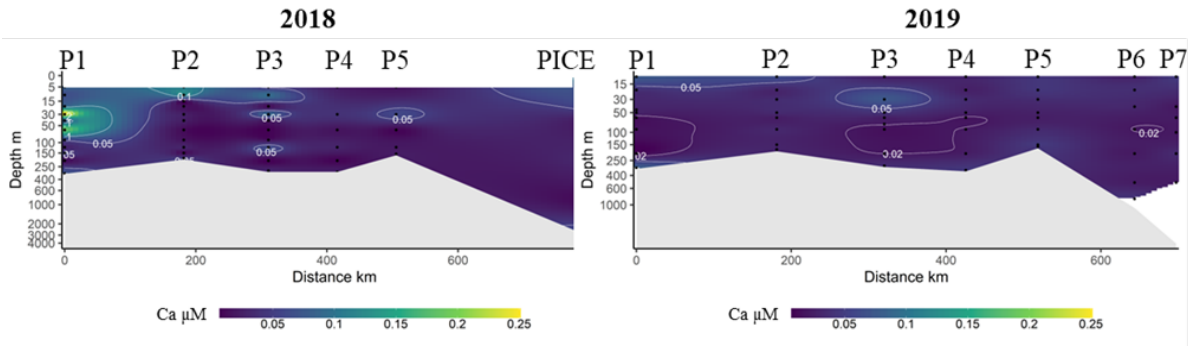

1

2

Figure A3: Concentration of particulate Calcium (Ca) in µM during August 2018 and August 2019 for all stations of the sampling transect from 76°N to 83°N (left to right). Black dots represent sampling points and the depth axis is in log scale.

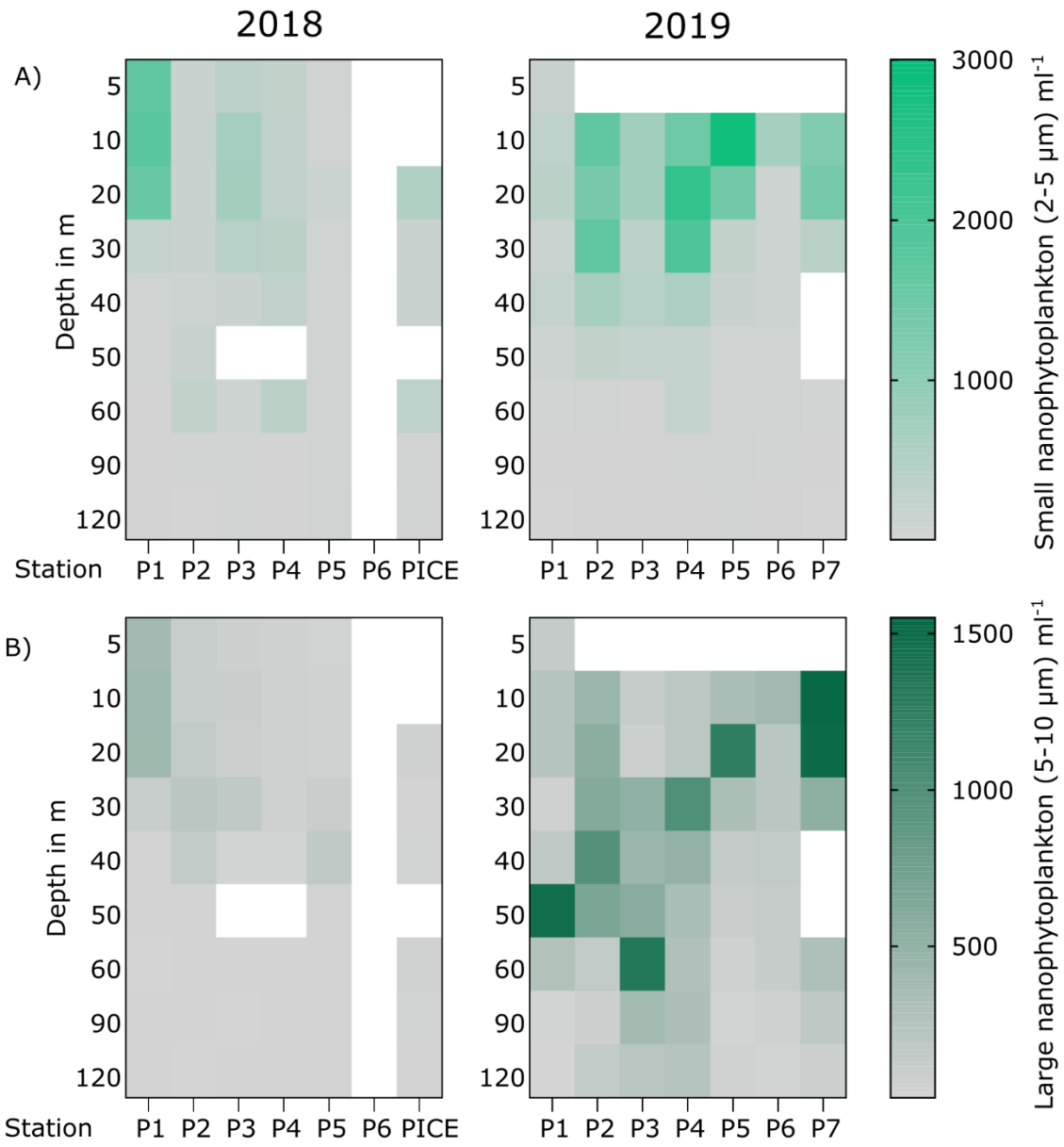

1

Figure A4: Heatmap showing for the upper 120 m of the water column abundances of A) small nanophytoplankton in cells mL^{-1} and B) small nanophytoplankton in cells mL^{-1}. White background indicates that samples were not taken. Scales are different for the different groups.

2

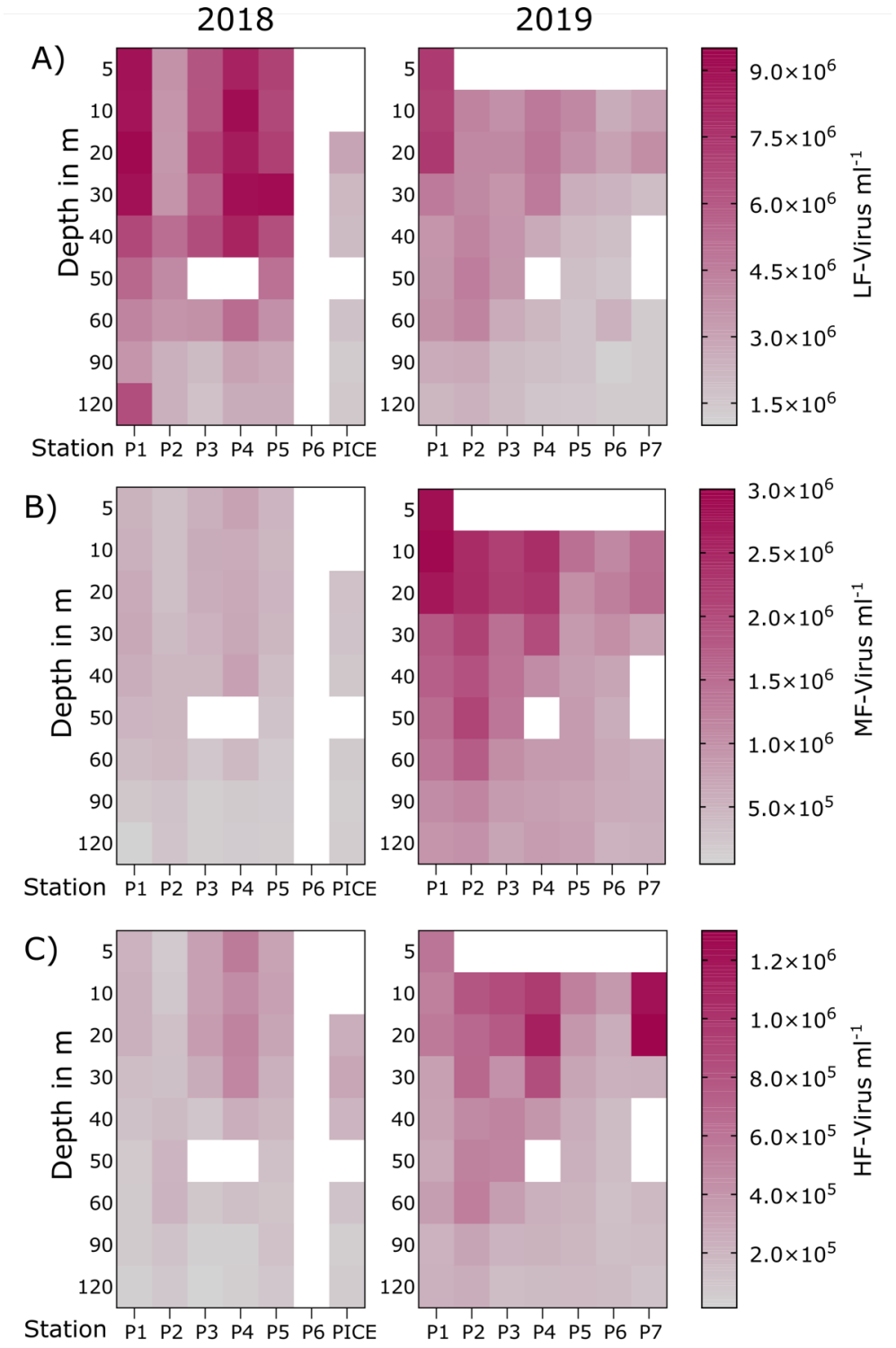

1

Figure A5: Heatmap showing for the upper 120 m of the water column abundances of A) small-sized virus in particles mL^{-1}, B) medium-sized virus in particles mL^{-1} and C) large-sized virus in particles mL^{-1}. White background indicates that samples were not taken. Scales are different for the different groups.

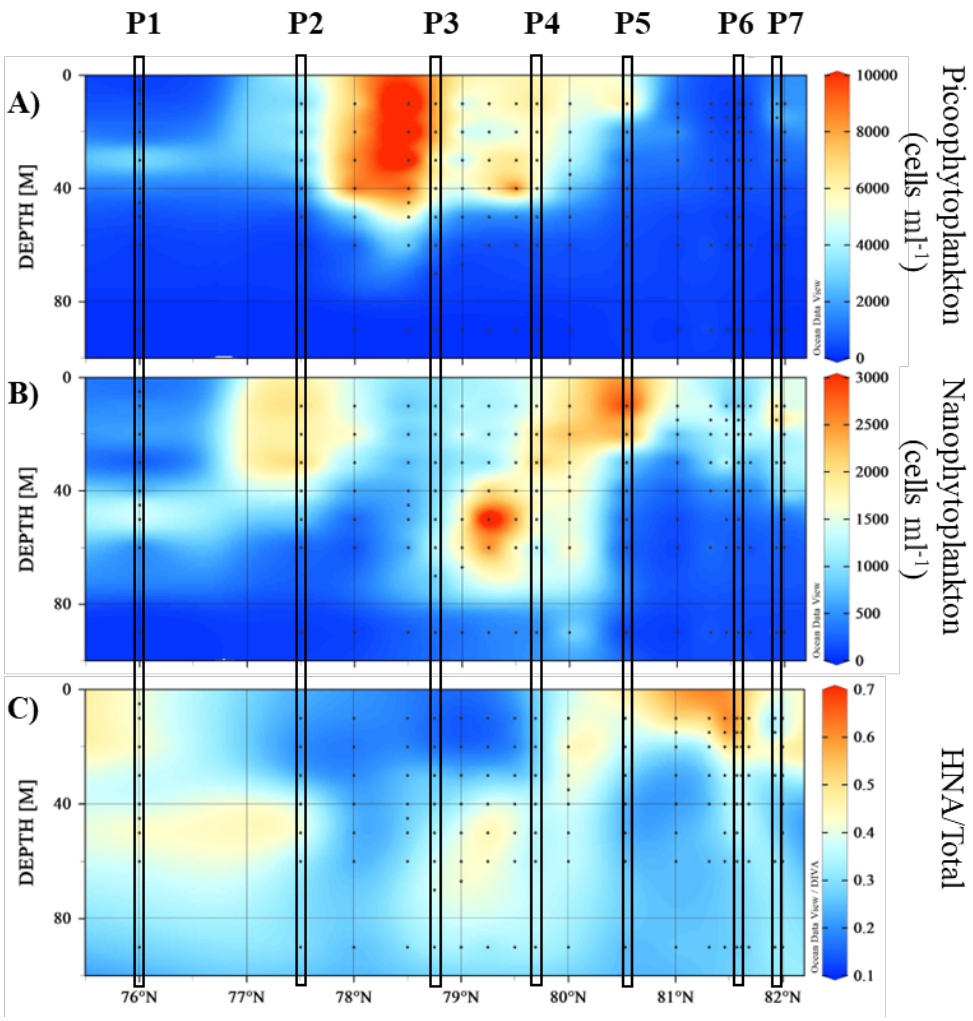

1

2

Figure A6: Abundance of different small phytoplankton groups; A) picophytoplankton (0.2-2 µm) and B) nanophytoplankton (2-10 µm). C) The ratio of the abundance of high nucleic acid containing bacteria (HNA) to total bacteria along the sampling transect in August 2019.

3

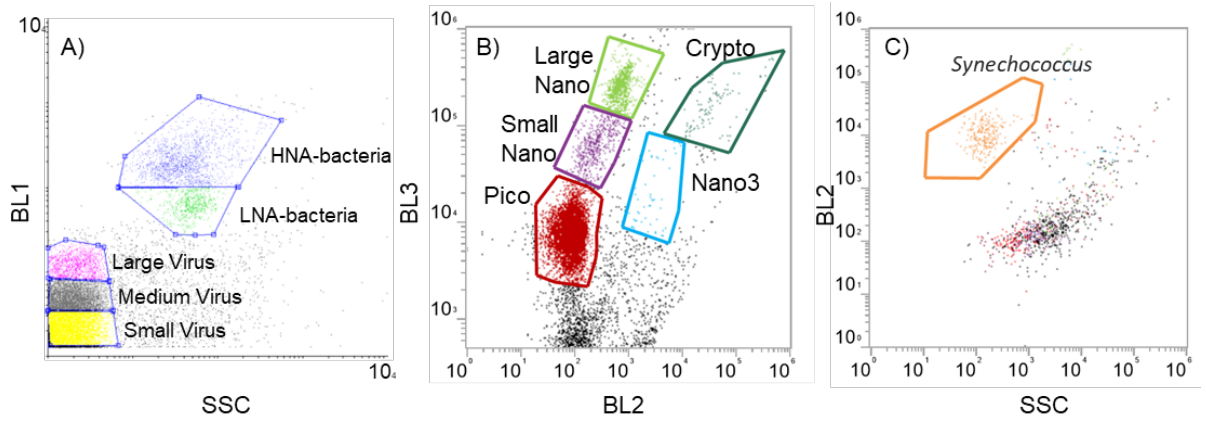

1

Figure A7: Biparametric flow cytometry plots with the applied grouping of the different A) bacterial groups, B) phytoplankton groups and C) *Synechococcus*. Different groups are indicated by the coloured frames according to their grouping on either A) BL1 (green fluorescence) vs. SSC (side scatter); B) BL3 (red fluorescence) vs. BL2 (orange fluorescence) and C) BL2 vs. SSC.

2

3

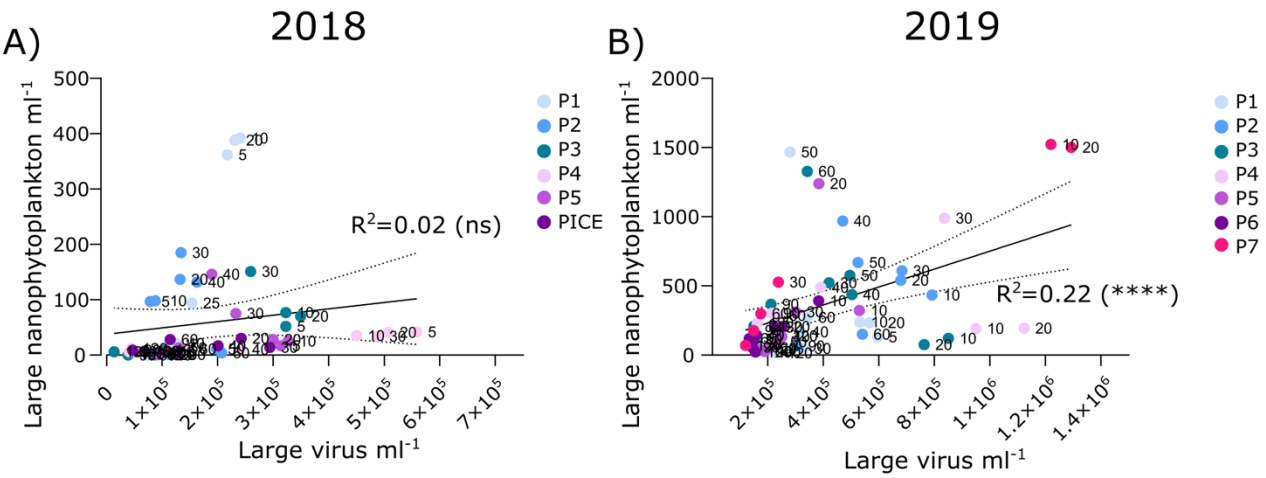

Figure A8: Linear regression analyses for A) 2018 and B) 2019 of large nanophytoplankton abundance against large virus abundance. Numbers next to data points indicate water depths in m.

References:

Ardyna, M., Arrigo, K.R., 2020. Phytoplankton dynamics in a changing Arctic Ocean. Nat. Clim. Change 2020 10:10 10, 892–903. https://doi.org/10.1038/s41558-020-0905-y

Armstrong, R.A., 2014. When to use the Bonferroni correction. Ophthalmic Physiol Opt 34, 502–508. https://doi.org/10.1111/OPO.12131

Arrigo, K.R., 2004. Marine microorganisms and global nutrient cycles. Nature 2005 437:7057 437, 349–355. https://doi.org/10.1038/nature04159

Arrigo, K.R., van Dijken, G.L., 2015. Continued increases in Arctic Ocean primary production. Prog Oceanogr 136, 60–70. https://doi.org/10.1016/J.POCEAN.2015.05.002

Årthun, M., Eldevik, T., Smedsrud, L.H., 2019. The role of atlantic heat transport in future Arctic winter sea ice loss. J Clim 32, 3327–3341. https://doi.org/10.1175/JCLI-D-18-0750.1

Årthun, M., Eldevik, T., Smedsrud, L.H., Skagseth, Ingvaldsen, R.B., 2012. Quantifying the influence of Atlantic heat on Barents Sea ice variability and retreat. J Clim 25, 4736–4743. https://doi.org/10.1175/JCLI-D-11-00466.1

Asbjørnsen, H., Årthun, M., Skagseth, Ø., Eldevik, T., 2020. Mechanisms underlying recent Arctic atlantification. Geophys Res Lett 47, e2020GL088036. https://doi.org/10.1029/2020GL088036

Assmy, P., Cecilie Kvernvik, A., Hop, H., Hoppe, C.J.M., Chierici, M., David T., D., Duarte, P., Fransson, A., García, L.M., Patuła, W., Kwaśniewski, S., Maturilli, M., Pavlova, O.,

Tatarek, A., Wiktor, J.M., Wold, A., Wolf, K.K.E., Bailey, A., 2023. Seasonal plankton dynamics in Kongsfjorden during two years of contrasting environmental conditions. Prog Oceanogr 213, 102996. https://doi.org/10.1016/J.POCEAN.2023.102996

Bienhold, C., Schourup-Kristensen, V., Krumpen, T., Nöthig, E.M., Wenzhöfer, F., Korhonen, M., Vredenborg, M., Hehemann, L., Boetius, A., 2022. Effects of sea ice retreat and ocean warming on the Laptev Sea continental slope ecosystem (1993 vs 2012). Front Mar Sci 9, 2587. https://doi.org/10.3389/FMARS.2022.1004959/BIBTEX

Bodur, Y., Marquardt, M., Dubourg, P., Amargant-Arumí, M., Reigstad, M., 2023a. Downward vertical flux of particulate organic carbon (POC) and nitrogen (PON) in the northern Barents Sea during August 2019, Nansen Legacy cruise 2019706 Q3. https://doi.org/10.11582/2023.00093

Bodur, Y., Marquardt, M., Dubourg, P., Dietrich, U., Svensen, C., Reigstad, M., 2023b. Downward vertical flux of particulate organic carbon (POC) and nitrogen (PON) in the northern Barents Sea during August 2018, Nansen Legacy cruise 2018707 J/C 1-2 . https://doi.org/https://doi.org/10.11582/2023.00092

Bonan, D.B., Lehner, F., Holland, M.M., 2021. Partitioning uncertainty in projections of Arctic sea ice. Environ Res Let. 16, 044002. https://doi.org/10.1088/1748-9326/ABE0EC

Bratbak, G., Skjoldal, E.F., Petelenz, E.A., 2022. Concentration of Particulate Organic Carbon (POC) from the sea water and sea ice in the northern Barents Sea as part of the Nansen Legacy project, Cruise 2018707, JC1_2; https://doi.org/10.11582/2022.00049 [WWW Document]. URL https://archive.sigma2.no/pages/public/datasetDetail.jsf?id=10.11582/2022.00049 (accessed 3.30.23).

Campbell, K., Matero, I., Bellas, C., Turpin-Jelfs, T., Anhaus, P., Graeve, M., Fripiat, F., Tranter, M., Landy, J.C., Sanchez-Baracaldo, P., Leu, E., Katlein, C., Mundy, C.J., Rysgaard, S., Tedesco, L., Haas, C., Nicolaus, M., 2022. Monitoring a changing Arctic: Recent advancements in the study of sea ice microbial communities. Ambio 51, 318–332. https://doi.org/10.1007/S13280-021-01658-Z/FIGURES/6

Carmack, E., Wassmann, P., 2006. Food webs and physical–biological coupling on pan-Arctic shelves: Unifying concepts and comprehensive perspectives. Prog Oceanogr 71, 446–477. https://doi.org/10.1016/J.POCEAN.2006.10.004

Chierici, M., Jones, E., Fransson, A., 2021a. Water column data on dissolved inorganic nutrients (nitrite, nitrate, phosphate and silicic acid) from the Nansen LEGACY joint cruise KH 2018707 with R.V. Kronprins Haakon, 8-20 August 2018.

Chierici, M., Jones, E., Lødemel, H.H., 2021b. Water column data on dissolved inorganic nutrients (nitrite, nitrate, phosphate and silicic acid) from the Nansen LEGACY seasonal cruise Q3, 2019706, with R.V. Kronprins Haakon, 5-27 August 2019.

Cota, G.F., Pomeroy, L.R., Harrison, W.G., Jones, E.P., Peters, F., Sheldon, W.M., Weingartner, T.R., 1996. Nutrients, primary production and microbial heterotrophy in the southeastern Chukchi Sea: Arctic summer nutrient depletion and heterotrophy. Mar Ecol Prog Ser 135, 247–258. https://doi.org/10.3354/MEPS135247

Csapó, H.K., Grabowski, M., Węsławski, J.M., 2021. Coming home - Boreal ecosystem claims Atlantic sector of the Arctic. Sci Total Environ 771, 144817. https://doi.org/10.1016/J.SCITOTENV.2020.144817

Dalpadado, P., Arrigo, K.R., Hjøllo, S.S., Rey, F., Ingvaldsen, R.B., Sperfeld, E., Van Dijken, G.L., Stige, L.C., Olsen, A., Ottersen, G., 2014. Productivity in the barents sea - response

to recent climate variability. PLoS One 9, e95273. https://doi.org/10.1371/JOURNAL.PONE.0095273
Dalpadado, P., Arrigo, K.R., van Dijken, G.L., Skjoldal, H.R., Bagøien, E., Dolgov, A. V., Prokopchuk, I.P., Sperfeld, E., 2020. Climate effects on temporal and spatial dynamics of phytoplankton and zooplankton in the Barents Sea. Prog Oceanogr 185, 102320. https://doi.org/10.1016/J.POCEAN.2020.102320
Dinasquet, J., Ortega-Retuerta, E., Lovejoy, C., Obernosterer, I., 2018. Editorial: microbiology of the rapidly changing polar environments. Front Mar Sci 0, 154. https://doi.org/10.3389/FMARS.2018.00154
Dong, K., Kvile, K.Ø., Stenseth, N.C., Stige, L.C., 2020. Associations among temperature, sea ice and phytoplankton bloom dynamics in the Barents Sea. Mar Ecol Prog Ser 635, 25–36. https://doi.org/10.3354/MEPS13218
Downes, P.P., 2022. The effects of changing sea ice conditions on microbial production and community composition in the Barents Sea. Doctoral thesis, University of Bristol, unpublished.
Dunse, T., Dong, K., Schanke Aas, K., Stige, L.C., 2022. Regional-scale phytoplankton dynamics and their association with glacier meltwater runoff in Svalbard. Biogeosciences 19, 271–294. https://doi.org/10.5194/bg-19-271-2022
Dybwad, C., Assmy, P., Olsen, L.M., Peeken, I., Nikolopoulos, A., Krumpen, T., Randelhoff, A., Tatarek, A., Wiktor, J.M., Reigstad, M., 2021. Carbon export in the seasonal sea ice zone north of Svalbard from winter to late summer. Front Mar Sci 7. https://doi.org/10.3389/fmars.2020.525800
Egge, J., Aksnes, D., 1992. Silicate as regulating nutrient in phytoplankton competition. Mar Ecol Prog Ser 83, 281–289.
Eich, C., Biggs, T.E.G., van de Poll, W.H., van Manen, M., Tian, H.A., Jung, J., Lee, Y., Middag, R., Brussaard, C.P.D., 2022. Ecological importance of viral lysis as a loss factor of phytoplankton in the Amundsen Sea. Microorganisms 10, 1967. https://doi.org/10.3390/MICROORGANISMS10101967/S1
Eicken, H., 2003. Sea ice: an introduction to its physics, biology, chemistry and geology. Biodivers Conserv 13, 1795–1796. https://doi.org/10.1023/b:bioc.0000029368.94861.47
Eilertsen, H.C., Tande, K.S., Taasen, J.P., 1989. Vertical distributions of primary production and grazing by *Calanus glacialis* (Jaschnov) and *C. hyperboreus* (Kroyer) in Arctic waters (Barents Sea). Polar Biol 9, 253–260.
Engelsen, O., Hegseth, E.N., Hop, H., Hansen, E., Falk-Petersen, S., 2002. Spatial variability of chlorophyll-a in the Marginal Ice Zone of the Barents Sea, with relations to sea ice and oceanographic conditions. J Mar Syst 35, 79–97. https://doi.org/10.1016/S0924-7963(02)00077-5
Erga, S.R., Haugen, S.B., Bratbak, G., Egge, J.K., Heldal, M., Mork, K.A., Norland, S., 2017. Seasonal variations in C:N:Si:Ca:P:Mg:S:K:Fe relationships of seston from Norwegian coastal water: Impact of extreme offshore forcing during winter-spring 2010. Mar Chem 196, 1–12. https://doi.org/10.1016/J.MARCHEM.2017.07.001
Fagerbakke, K.M., Heldal, M., Norland, S., Heimdal, B.R., Båtvik, H., 2012. *Emiliania huxleyi*. Chemical composition and size of coccoliths from enclosure experiments and a Norwegian fjord. Mar Biol Res 79, 349–355. https://doi.org/10.1080/00364827.1994.10413566

Grasshoff, K., Kremling, K., Ehrhardt, M., 1978. Methods of seawater analysis, Third Edition, Marine Chemistry.
Greenwood, N.N., Earnshaw, A., 2012. Chemistry of the elements, Second Edition.
Gundersen, K., Møgster, J.S., Lien, V.S., Ershova, E., Lunde, L.F., Arnesen, H., Olsen, A.K., 2022. Thirty years of nutrient biogeochemistry in the Barents Sea and the adjoining arctic ocean, 1990–2019. Scientific Data 2022 9:1 9, 1–12. https://doi.org/10.1038/s41597-022-01781-w
Hegseth, E.N., Sundfjord, A., 2008. Intrusion and blooming of Atlantic phytoplankton species in the high Arctic. J Mar Syst 74. https://doi.org/10.1016/j.jmarsys.2007.11.011
Hill, V., Cota, G., 2005. Spatial patterns of primary production on the shelf, slope and basin of the Western Arctic in 2002. Deep Sea Res Part II Top Stud Oceanogr 52, 3344–3354. https://doi.org/10.1016/J.DSR2.2005.10.001
Howard-Jones, M.H., Ballard, V.D., Allen, A.E., Frischer, M.E., Verity, P.G., 2002a. Distribution of bacterial biomass and activity in the marginal ice zone of the central Barents Sea during summer. J Mar Syst 38, 77–91. https://doi.org/10.1016/S0924-7963(02)00170-7
Hudier, E., Ingram, G., 1994. Small-scale melt processes governing the flushing of nutrients from a first-year sea-ice, Hudson-Bay, canada. *Ocean acta* 17, 397–403.
Hunt, G.L., Blanchard, A.L., Boveng, P., Dalpadado, P., Drinkwater, K.F., Eisner, L., Hopcroft, R.R., Kovacs, K.M., Norcross, B.L., Renaud, P., Reigstad, M., Renner, M., Skjoldal, H.R., Whitehouse, A., Woodgate, R.A., 2013. The Barents and Chukchi Seas: Comparison of two Arctic shelf ecosystems J Mar Syst 109–110, 43–68. https://doi.org/10.1016/J.JMARSYS.2012.08.003
Ingvaldsen, R., Bluhm, B., Aberle-Malzahn, N., Amundsen, R., Ardelan, M. Van, Bagøien, E., Bratbak, G., Bratrein, M., Chierici, M., Descoteux, R., Dietrich, U., Divine, D., Ellingsen, P.G., Fransson, A., Halvorsen, E., Hoff, S., Holm, E., Jentoft, S., Jones, E., Jørgensen, L., Pedersen, R., Sanchez, N., Skjoldal, E., Stige, L.C., Stippkugel, A., Seim, S., Supraha, L., Steinsland, A., Svensen, C., Vader, A., Vieweg, I., Vonnahme, T., Åström, E., 2020. Joint Cruise 1-2 2018. The Nansen Legacy Report Series. https://doi.org/10.7557/NLRS.5628
Ingvaldsen, R., Loeng, H., 2009. Ecosystem Barents Sea: Physical oceanography , in: Ecosystem Barents Sea. pp. 33–64.
Ingvaldsen, R.B., 2022. CTD data from Nansen Legacy Cruise - Joint cruise 1-2; https://doi.org/10.21335/NMDC-714672628 [WWW Document]. URL http://metadata.nmdc.no/metadata-api/landingpage/95a8975ffeae330eefc8ae5c113ea6c8 (accessed 3.30.23).
Ingvaldsen, R.B., Assmann, K.M., Primicerio, R., Fossheim, M., Polyakov, I. V., Dolgov, A. V., 2021. Physical manifestations and ecological implications of Arctic Atlantification. Nat Rev Earth Environ. https://doi.org/10.1038/s43017-021-00228-x
Isaksen, K., Nordli, Ø., Ivanov, B., Køltzow, M.A.Ø., Aaboe, S., Gjelten, H.M., Mezghani, A., Eastwood, S., Førland, E., Benestad, R.E., Hanssen-Bauer, I., Brækkan, R., Sviashchennikov, P., Demin, V., Revina, A., Karandasheva, T., 2022. Exceptional warming over the Barents area. Sci Rep 12. https://doi.org/10.1038/s41598-022-13568-5
Iversen, K.R., Seuthe, L., 2011. Seasonal microbial processes in a high-latitude fjord (Kongsfjorden, Svalbard): I. Heterotrophic bacteria, picoplankton and nanoflagellates. Polar Biol 34, 731–749. https://doi.org/10.1007/S00300-010-0929-2/TABLES/6

Iversen, M.H., 2023. Carbon export in the ocean: a biologist's perspective. Annu Rev Mar Sci 15, 357–381. https://doi.org/10.1146/ANNUREV-MARINE-032122-035153

Kahru, M., Lee, Z., Mitchell, B.G., Nevison, C.D., 2016. Effects of sea ice cover on satellite-detected primary production in the Arctic Ocean. Biol Lett 12. https://doi.org/10.1098/RSBL.2016.0223

Kirchman, D.L., Hill, V., Cottrell, M.T., Gradinger, R., Malmstrom, R.R., Parker, A., 2009a. Standing stocks, production, and respiration of phytoplankton and heterotrophic bacteria in the western Arctic Ocean. Deep Sea Res Part II Top Stud Oceanogr 56, 1237–1248. https://doi.org/10.1016/J.DSR2.2008.10.018

Kirchman, D.L., Morán, X.A.G., Ducklow, H., 2009b. Microbial growth in the polar oceans - Role of temperature and potential impact of climate change. Nat Rev Microbiol 7, 451–459. https://doi.org/10.1038/nrmicro2115

Kohlbach, D., Goraguer, L., Bodur, Y. V., Müller, O., Amargant-Arumí, M., Blix, K., Bratbak, G., Chierici, M., Dąbrowska, A.M., Dietrich, U., Edvardsen, B., García, L.M., Gradinger, R., Hop, H., Jones, E., Lundesgaard, Ø., Olsen, L.M., Reigstad, M., Saubrekka, K., Tatarek, A., Wiktor, J.M., Wold, A., Assmy, P., 2023. Earlier sea-ice melt extends the oligotrophic summer period in the Barents Sea with low algal biomass and associated low vertical flux. Prog Oceanogr 213, 103018. https://doi.org/10.1016/J.POCEAN.2023.103018

Kranzler, C.F., Krause, J.W., Brzezinski, M.A., Edwards, B.R., Biggs, W.P., Maniscalco, M., McCrow, J.P., Van Mooy, B.A.S., Bidle, K.D., Allen, A.E., Thamatrakoln, K., 2019. Silicon limitation facilitates virus infection and mortality of marine diatoms. Nature Microbiology 2019 4:11 4, 1790–1797. https://doi.org/10.1038/s41564-019-0502-x

Krumhardt, K.M., Lovenduski, N.S., Iglesias-Rodriguez, M.D., Kleypas, J.A., 2017. Coccolithophore growth and calcification in a changing ocean. Prog Oceanogr 159, 276–295. https://doi.org/10.1016/J.POCEAN.2017.10.007

Langer, M.R., 2008. Assessing the Contribution of Foraminiferan Protists to Global Ocean Carbonate Production. J Eukaryot Microbiol 55, 163–169. https://doi.org/10.1111/J.1550-7408.2008.00321.X

Larsen, A., Egge, J.K., Nejstgaard, J.C., Di Capua, I., Thyrhaug, R., Bratbak, G., Thingstad, T.F., 2015. Contrasting response to nutrient manipulation in Arctic mesocosms are reproduced by a minimum microbial food web model. Limnol Oceanogr 60, 360-374. https://doi.org/10.1002/lno.10025

Larsen, J.B., Larsen, A., Thyrhaug, R., Bratbak, G., Sandaa, R.A., 2008. Response of marine viral populations to a nutrient induced phytoplankton bloom at different pCO 2 levels. Biogeosciences, 5(2), pp.523-533. https://doi.org/10.5194/bg-5-523-2008

Legacy, T.N., 2022. Nansen Legacy Sampling Protocols v10. The Nansen Legacy Report Series. https://doi.org/10.7557/NLRS.6684

Lewis, K.M., Van Dijken, G.L., Arrigo, K.R., 2020. Changes in phytoplankton concentration now drive increased Arctic Ocean primary production. Science (1979) 369, 198–202. https://doi.org/10.1126/SCIENCE.AAY8380/SUPPL_FILE/AAY8380-LEWIS-SM.PDF

Lind, S., Ingvaldsen, R.B., Furevik, T., 2018. Arctic warming hotspot in the northern Barents Sea linked to declining sea-ice import. Nature Climate Change 2018 8:7 8, 634–639. https://doi.org/10.1038/s41558-018-0205-y

Litchman, E., Klausmeier, C.A., Schofield, O.M., Falkowski, P.G., 2007. The role of functional traits and trade-offs in structuring phytoplankton communities: Scaling from cellular to ecosystem level. Ecol Lett 10, 1170–1181. https://doi.org/10.1111/J.1461-0248.2007.01117.X

Marie, D., Brussaard, C.P.D., Thyrhaug, R., Bratbak, G., Vaulot, D., 1999. Enumeration of marine viruses in culture and natural samples by flow cytometry. Appl Environ Microbiol 65, 45–52.

Marquardt, M., Bodur, Y. V., Dubourg, P., Reigstad, M., 2022. Concentration of Particulate Organic Carbon (POC) and Particulate Organic Nitrogen (PON) from the sea water and sea ice in the northern Barents Sea as part of the Nansen Legacy project, Cruise 2019706 Q3; https://doi.org/10.11582/2022.00055 [WWW Document]. URL https://archive.sigma2.no/pages/public/datasetDetail.jsf?id=10.11582/2022.00055 (accessed 3.30.23).

Martin, J.H., Knauer, G.A., Karl, D.M., Broenkow, W.W., 1987. VERTEX: carbon cycling in the northeast Pacific. Deep Sea Res Part I Oceanogr Res Pap 34, 267–285. https://doi.org/10.1016/0198-0149(87)90086-0

Matrai, P., Vernet, M., Wassmann, P., 2007. Relating temporal and spatial patterns of DMSP in the Barents Sea to phytoplankton biomass and productivity. J Mar Syst 67, 83–101. https://doi.org/10.1016/J.JMARSYS.2006.10.001

McLaughlin, F.A., Carmack, E.C., 2010. Deepening of the nutricline and chlorophyll maximum in the Canada Basin interior, 2003–2009. Geophys Res Lett 37, 24602. https://doi.org/10.1029/2010GL045459

Moran, M.A., Belas, R., Schell, M.A., González, J.M., Sun, F., Sun, S., Binder, B.J., Edmonds, J., Ye, W., Orcutt, B., Howard, E.C., Meile, C., Palefsky, W., Goesmann, A., Ren, Q., Paulsen, I., Ulrich, L.E., Thompson, L.S., Saunders, E., Buchan, A., 2007. Ecological genomics of marine Roseobacters. Appl Environ Microbiol 73, 4559. https://doi.org/10.1128/AEM.02580-06

Müller, O., Olsen, L.M., Skjoldal, E.F., Stabell, H., Våge, S., Bratbak, G., 2023a. Bacterial production measurements (rate of production of biomass expressed as carbon by prokaryotes [bacteria and archaea]) during Nansen Legacy Cruises. https://doi.org/https://doi.org/10.21335/NMDC-1815353537

Müller, O., Petelenz, E., Tsagkaraki, T., Langvad, M., Olsen, L., Grytaas, A., Thiele, S., Stabell, H., Skjoldal, E., Våge, S., Bratbak, G., 2023b. Flow cytometry measurements (abundance of virus, bacteria and small protists (primarily <20µm)) during Nansen Legacy cruises. https://doi.org/https://doi.org/10.21335/NMDC-1588963816

Müller, O., Seuthe, L., Pree, B., Bratbak, G., Larsen, A., Paulsen, M.L., 2021. How microbial food web interactions shape the arctic ocean bacterial community revealed by size fractionation experiments. Microorganisms 9, 2378. https://doi.org/10.3390/MICROORGANISMS9112378

Nøst Hegseth, E., 1998. Primary production of the northern Barents Sea. Polar Res 17, 113–123. https://doi.org/10.3402/polar.v17i2.6611

Nummelin, A., Ilicak, M., Li, C., Smedsrud, L.H., 2016. Consequences of future increased Arctic runoff on Arctic Ocean stratification, circulation, and sea ice cover. J Geophys Res Oceans 121, 617–637. https://doi.org/10.1002/2015JC011156

Oksanen, J., Blanchet, F.G., Friendly, M., Kindt, R., Legendre, P., Mcglinn, D., Minchin, P.R., O'hara, R.B., Simpson, G.L., Solymos, P., Henry, M., Stevens, H., Szoecs, E., Maintainer, H.W., 2022. vegan: Community Ecology Package, version 2.5-7. ci.nii.ac.jp.

Olli, K., Wexels Riser, C., Wassmann, P., Ratkova, T., Arashkevich, E., Pasternak, A., 2002. Seasonal variation in vertical flux of biogenic matter in the marginal ice zone and the central Barents Sea. J Mar Syst 38, 189–204. https://doi.org/10.1016/S0924-7963(02)00177-X

Orkney, A., Platt, T., Narayanaswamy, B.E., Kostakis, I., Bouman, H.A., 2020. Bio-optical evidence for increasing *Phaeocystis* dominance in the Barents Sea: Increasing *Phaeocystis* in Barents Sea. Philos Trans Royal Soc 378. https://doi.org/10.1098/rsta.2019.0357

Orkney, A., Sathyendranath, S., Jackson, T., Porter, M., Bouman, H.A., 2022. Atlantic inflow is the primary driver of remotely sensed autumn blooms in the Barents Sea. Mar Ecol Prog Ser 701, 25–40. https://doi.org/10.3354/MEPS14201

OSI SAF Sea ice index 1978-onwards, version 2.2 (2023), OSI-420. EUMETSAT Ocean and Sea Ice Satellite Application Facility. Data extracted from https://cryo.met.no/en/sea-ice-index-bar (2018-2019) (Barents Sea) accessed 5th October 2023.

Oziel, L., Baudena, A., Ardyna, M., Massicotte, P., Randelhoff, A., Sallée, J.B., Ingvaldsen, R.B., Devred, E., Babin, M., 2020. Faster Atlantic currents drive poleward expansion of temperate phytoplankton in the Arctic Ocean. Nat Commun 11. https://doi.org/10.1038/s41467-020-15485-5

Oziel, L., Neukermans, G., Ardyna, M., Lancelot, C., Tison, J.L., Wassmann, P., Sirven, J., Ruiz-Pino, D., Gascard, J.C., 2017. Role for Atlantic inflows and sea ice loss on shifting phytoplankton blooms in the Barents Sea. J Geophys Res Oceans 122. https://doi.org/10.1002/2016JC012582

Paulino, A.I., Heldal, M., Norland, S., Egge, J.K., 2013. Elemental stoichiometry of marine particulate matter measured by wavelength dispersive X-ray fluorescence (WDXRF) spectroscopy. J Mar Biol Assoc U. K. 93, 2003–2014. https://doi.org/10.1017/S0025315413000635

Paulsen, M.L., Doré, H., Garczarek, L., Seuthe, L., Müller, O., Sandaa, R.-A., Bratbak, G., Larsen, A., 2016. *Synechococcus* in the Atlantic gateway to the Arctic Ocean. Front Mar Sci 3. https://doi.org/10.3389/fmars.2016.00191

Piontek, J., Galgani, L., Nöthig, E.M., Peeken, I., Engel, A., 2021. Organic matter composition and heterotrophic bacterial activity at declining summer sea ice in the central Arctic Ocean. Limnol Oceanogr 66, S343–S362. https://doi.org/10.1002/LNO.11639

Polyakov, I. V., Alkire, M.B., Bluhm, B.A., Brown, K.A., Carmack, E.C., Chierici, M., Danielson, S.L., Ellingsen, I., Ershova, E.A., Gårdfeldt, K., Ingvaldsen, R.B., Pnyushkov, A. V., Slagstad, D., Wassmann, P., 2020. Borealization of the Arctic Ocean in response to anomalous advection from Sub-Arctic seas. Front Mar Sci 7, 491. https://doi.org/10.3389/FMARS.2020.00491/BIBTEX

Polyakov, I. V., Pnyushkov, A. V., Alkire, M.B., Ashik, I.M., Baumann, T.M., Carmack, E.C., Goszczko, I., Guthrie, J., Ivanov, V. V., Kanzow, T., Krishfield, R., Kwok, R., Sundfjord, A., Morison, J., Rember, R., Yulin, A., 2017. Greater role for Atlantic inflows on sea-ice loss in the Eurasian Basin of the Arctic Ocean. Science (1979) 356, 285–291. https://doi.org/10.1126/SCIENCE.AAI8204

Pomeroy, L.R., Wiebe, W.J., Deibel, D., Thompson, R.J., Rowe, G.T., Pakulski, J.D., 1991. Bacterial responses to temperature and substrate concentration during the Newfoundland spring bloom. Mar Ecol Prog Ser 75, 143–159. https://doi.org/10.3354/meps075143

Rantanen, M., Karpechko, A.Y., Lipponen, A., Nordling, K., Hyvärinen, O., Ruosteenoja, K., Vihma, T., Laaksonen, A., 2022. The Arctic has warmed nearly four times faster than the globe since 1979. Commun Earth Environ 2022 3:1 3, 1–10. https://doi.org/10.1038/s43247-022-00498-3

Rat'kova, T.N., Wassmann, P., 2002a. Seasonal variation and spatial distribution of phyto- and protozooplankton in the central Barents Sea J Mar Syst 38, 47–75. https://doi.org/10.1016/S0924-7963(02)00169-0

Reigstad, M., 2022. CTD data from Nansen Legacy Cruise - Seasonal cruise Q3; https://doi.org/10.21335/NMDC-1107597377 [WWW Document]. URL http://metadata.nmdc.no/metadata-api/landingpage/e540a99696cba051d5a39342e8bf1954 (accessed 3.30.23).

Reigstad, M., Gabrielsen, T., Amargant, M., Amundsen, R., Bluhm, B., Bodur, Y., Bremnes, J., Brun, N., Dalpadado, P., Dmoc, K., Edvardsen, B., Garnett, J., Gawinski, C., Giebichenstein, J., Haarr, A., Hoff, S., Jorda, E., Karlsson, K., Kohler, S., Leithe, J., Marquardt, M., Morel, C., Müller, O., Liholt, H.N., Vidar Nordstrand, J., Nowicki, R., Olsen, L., Anglada Ortiz, G., Pedersen, R., Sanchez, N., Saubrekka, K., Sen, A., Christian Stige, L., Stippkugel, A., Vader, A., Wold, A., 2022. Seasonal Cruise Q3. The Nansen Legacy Report Series. https://doi.org/10.7557/NLRS.6407

Reigstad, M., Wassmann, P., Wexels Riser, C., Øygarden, S., Rey, F., 2002. Variations in hydrography, nutrients and chlorophyll a in the marginal ice-zone and the central Barents Sea. J Mar Syst 38, 9–29. https://doi.org/10.1016/S0924-7963(02)00167-7

Reigstad, M., Wexels Riser, C., Wassmann, P., Ratkova, T., 2008. Vertical export of particulate organic carbon: Attenuation, composition and loss rates in the northern Barents Sea. Deep Sea Res Part II Top Stud Oceanogr 55, 2308–2319. https://doi.org/10.1016/J.DSR2.2008.05.007

Rich, J., Gosselin, M., Sherr, E., Sherr, B., Kirchman, D.L., 1997. High bacterial production, uptake and concentrations of dissolved organic matter in the Central Arctic Ocean. Deep Sea Res Part II Top Stud Oceanogr 44, 1645–1663. https://doi.org/10.1016/S0967-0645(97)00058-1

Rieke, O., Årthun, M., Dörr, J.S., 2022. Rapid Sea Ice Changes in the Future Barents Sea. EGUsphere [preprint]. https://doi.org/10.5194/egusphere-2022-324

Rogge, A., Janout, M., Loginova, N., Trudnowska, E., Hörstmann, C., Wekerle, C., Oziel, L., Schourup-Kristensen, V., Ruiz-Castillo, E., Schulz, K., Povazhnyy, V. V., Iversen, M.H., Waite, A.M., 2022. Carbon dioxide sink in the Arctic Ocean from cross-shelf transport of dense Barents Sea water. Nature Geosci. 2022 16:1 16, 82–88. https://doi.org/10.1038/s41561-022-01069-z

Sakshaug, E., Johnsen, G., Andresen, K., Vernet, M., 1991. Modeling of light-dependent algal photosynthesis and growth: experiments with the Barents sea diatoms *Thalassiosira nordenskioldii* and *Chaetoceros furcellatus*. Deep Sea Res Part I Oceanogr Res Pap 38, 415–430. https://doi.org/10.1016/0198-0149(91)90044-G

Sakshaug, E., Johnsen, G., Kovacs, K., 2009. Ecosystem Barents Sea. Tapir Academic Press, Trondheim.

Sapp, M., Wichels, A., Wiltshire, K.H., Gerdts, G., 2007. Bacterial community dynamics during the winter-spring transition in the North Sea. FEMS Microbiol Ecol 59, 622–637. https://doi.org/10.1111/j.1574-6941.2006.00238.x

Seymour, J.R., Amin, S.A., Raina, J.B., Stocker, R., 2017. Zooming in on the phycosphere: The ecological interface for phytoplankton-bacteria relationships. Nat Microbiol https://doi.org/10.1038/nmicrobiol.2017.65

Signorini, S.R., McClain, C.R., 2009. Environmental factors controlling the Barents Sea spring-summer phytoplankton blooms. Geophys Res Lett 36. https://doi.org/10.1029/2009GL037695

Silva, E., Counillon, F., Brajard, J., Korosov, A., Pettersson, L.H., Samuelsen, A., Keenlyside, N., 2021. Twenty-one years of phytoplankton bloom phenology in the Barents, Norwegian, and North seas. Front Mar Sci 8, 1626. https://doi.org/10.3389/FMARS.2021.746327/BIBTEX

Simon, M., Azam, F., 1989. Protein content and protein synthesis rates of planktonic marine bacteria. Mar Ecol Prog Ser. https://doi.org/10.3354/meps051201

Skjoldal, H.R., Rey, F., 1989. Pelagic production and variability of the Barents Sea ecosystem, in: Biomass Yields and Geography of Large Marine Ecosystems. AAAS Selected Symposium 111. Routledge, pp. 241–286. https://doi.org/10.4324/9780429043406-9

Slagstad, D., Wassmann, P.F.J., Ellingsen, I., 2015. Physical constrains and productivity in the future Arctic Ocean. Front Mar Sci 2, 85. https://doi.org/10.3389/FMARS.2015.00085/BIBTEX

Smith, D.C., Azam, F., 1992. A simple, economical method for measuring bacterial protein synthesis rates in seawater using 3H-leucine 1. Mar. Microb. Food Webs 6, 107–114.

Steward, G.F., Smith, D.C., Azam, F., 1996. Abundance and production of bacteria and viruses in the Bering and Chukchi Seas. Mar Ecol Prog Ser 131, 287–300. https://doi.org/10.3354/MEPS131287

Strass, V.H., Nöthig, E.M., 1996. Seasonal shifts in ice edge phytoplankton blooms in the Barents Sea related to the water column stability. Polar Biol 16, 409–422. https://doi.org/10.1007/BF02390423/METRICS

Sturluson, M., Gissel Nielsen, T., Wassmann, P., 2008. Bacterial abundance, biomass and production during spring blooms in the northern Barents Sea. Deep Sea Res Part II Top Stud Oceanogr 55, 2186–2198. https://doi.org/10.1016/J.DSR2.2008.05.001

Sundfjord, A., Assmann, K.M., Lundesgaard, Ø., Renner, A.H.H., Lind, S., Ingvaldsen, R.B., 2020. Suggested water mass definitions for the central and northern Barents Sea, and the adjacent Nansen Basin. The Nansen Legacy Report Series. https://doi.org/10.7557/NLRS.5707

Sverdrup, H.U., 1953. On conditions for the vernal blooming of phytoplankton. ICES J Mar Sci 18, 287–295. https://doi.org/10.1093/icesjms/18.3.287

Thiele, S., Vader, A., Thomson, S., Saubrekka, K., Petelenz, E., Armo, H., Müller, O., Olsen, L., Bratbak, G., Øvreås, L., 2023. The summer bacterial and archaeal community composition of the northern Barents Sea. Prog Ocean 214, 103054. https://doi.org/10.1016/j.pocean.2023.103054

Thingstad, T.F., 2020. How trophic cascades and photic zone nutrient content interact to generate basin-scale differences in the microbial food web. ICES J Mar Sci 77, 1639-1647. https://doi.org/10.1093/icesjms/fsaa028

Thingstad, T.F., Krom, M.D., Mantoura, R.F.C., Flaten, C.A.F., Groom, S., Herut, B., Kress, N., Law, C.S., Pasternak, A., Pitta, P., Psarra, S., Rassoulzadegan, F., Tanaka, T., Tselepides, A., Wassmann, P., Woodward, E.M.S., Riser, C.W., Zodiatis, C., Zohary, T., 2005. Nature of phosphorus limitation in the ultraoligotrophic eastern Mediterranean. Science (1979) 309, 1068–1071. https://doi.org/10.1126/science.1112632

Tsagkaraki, T., Østgaard, H., Müller, O., Olsen, L.M., Ntinou, I., Thiele, S., Grytaas, A., Bratbak, G., 2023. Elemental concentration measurements (Na, Mg, Si, P, S, K, Ca, Mn,

Fe, Zn) of particulate matter using XRF (X-ray fluorescence) analysis during Nansen Legacy Cruises. https://doi.org/https://doi.org/10.21335/NMDC-1663991306
Uchimiya, M., Motegi, C., Nishino, S., Kawaguchi, Y., Inoue, J., Ogawa, H., Nagata, T., 2016. Coupled response of bacterial production to a wind-induced fall phytoplankton bloom and sediment resuspension in the Chukchi sea shelf, Western Arctic Ocean. Front Mar Sci 3, 231. https://doi.org/10.3389/FMARS.2016.00231/BIBTEX
Ugalde, S.C., Martin, A., Meiners, K.M., McMinn, A., Ryan, K.G., 2014. Extracellular organic carbon dynamics during a bottom-ice algal bloom (Antarctica). Aquat. Microb. Ecol. 73, 195–210. https://doi.org/10.3354/AME01717
Vader, A., Marquardt, M., Bodur, Y., 2021. Chlorophyll A and phaeopigments, Nansen Legacy; https://doi.org/10.21335/NMDC-1371694848.
Venables, W., Ripley, B., 2018. Modern Applied Statistics with S, Fourth edition 169. Springer New York, New York.
Verity, P.G., Wassmann, P., Frischer, M.E., Howard-Jones, M.H., Allen, A.E., 2002. Grazing of phytoplankton by microzooplankton in the Barents Sea during early summer. J Mar Syst 38, 109–123. https://doi.org/10.1016/S0924-7963(02)00172-0
von Appen, W.J., Waite, A.M., Bergmann, M., Bienhold, C., Boebel, O., Bracher, A., Cisewski, B., Hagemann, J., Hoppema, M., Iversen, M.H., Konrad, C., Krumpen, T., Lochthofen, N., Metfies, K., Niehoff, B., Nöthig, E.M., Purser, A., Salter, I., Schaber, M., Scholz, D., Soltwedel, T., Torres-Valdes, S., Wekerle, C., Wenzhöfer, F., Wietz, M., Boetius, A., 2021. Sea-ice derived meltwater stratification slows the biological carbon pump: results from continuous observations. Nature Communications 2021 12:1 12, 1–16. https://doi.org/10.1038/s41467-021-26943-z
Wassmann, P., 2011. Arctic marine ecosystems in an era of rapid climate change. Prog. Oceanogr. 90, 1–17. https://doi.org/10.1016/J.POCEAN.2011.02.002
Wassmann, P., 2002a. Seasonal C-cycling variability in the open and ice-covered waters of the Barents Sea: An introduction. J Mar Syst 38, 1–7. https://doi.org/10.1016/S0924-7963(02)00166-5
Wassmann, P., Ratkova, T., Andreassen, I., Vernet, M., Pedersen, G., Rey, F., 1999. Spring bloom development in the marginal ice zone and the central Barents Sea. Mar. Ecol. 20, 321–346. https://doi.org/10.1046/J.1439-0485.1999.2034081.X
Wassmann, P., Reigstad, M., Haug, T., Rudels, B., Carroll, M.L., Hop, H., Gabrielsen, G.W., Falk-Petersen, S., Denisenko, S.G., Arashkevich, E., Slagstad, D., Pavlova, O., 2006. Food webs and carbon flux in the Barents Sea. Prog. Oceanogr. 71, 232–287. https://doi.org/10.1016/J.POCEAN.2006.10.003
Wiedmann, I., Ceballos-Romero, E., Villa-Alfageme, M., Renner, A.H.H., Dybwad, C., van der Jagt, H., Svensen, C., Assmy, P., Wiktor, J.M., Tatarek, A., Różańska-Pluta, M., Iversen, M.H., 2020. Arctic observations identify phytoplankton community composition as driver of carbon flux attenuation. Geophys Res Lett 47, e2020GL087465. https://doi.org/10.1029/2020GL087465
Wiedmann, I., Reigstad, M., Sundfjord, A., Basedow, S., 2014. Potential drivers of sinking particle's size spectra and vertical flux of particulate organic carbon (POC): Turbulence, phytoplankton, and zooplankton. J Geophys Res Oceans 119, 6900–6917. https://doi.org/10.1002/2013JC009754
Zhang, F., Lin, L., Gao, Y., Cao, S., He, J., 2016. Ecophysiology of picophytoplankton in different water masses of the northern Bering Sea. Polar Biol 39, 1381–1397. https://doi.org/10.1007/S00300-015-1860-3/FIGURES/5

Zubkov, M.V., Burkill, P.H., Topping, J.N., 2007. Flow cytometric enumeration of DNA-stained oceanic planktonic protists. J Plankt Res 29(1), pp.79-86. https://doi.org/ 10.1093/plankt/fbl059